Quaternary Geology of the San Bernardino Mountains and their tectonic margins

Doug Yule[1] and James Spotila[2]
[1]*Department of Geological Sciences, California State University, Northridge, California 91330-8266, USA*
[2]*Department of Geosciences, Virginia Tech, Blacksburg, VA, 24061*

ABSTRACT

This trip will visit key sites that illustrate the temporal and spatial Quaternary geologic evolution of the San Bernardino Mountains. The Quaternary record here reveals a compelling story of fault reorganization, uplift, and erosion related to oblique convergence at the southern 'Big Bend' of the San Andreas fault. The currently active and several abandoned strands of the San Andreas fault bound the range on the southwest. Here, the fault-bounded Yucaipa Ridge block experienced >5 mm/yr of denudation from 0.5 to 0.8 Ma. Other structural blocks in the mountain range have experienced distinct uplift and erosion histories that will be explored. In San Gorgonio Pass, an ongoing debate about the seismic hazard facing southern California centers on whether through-going rupture of the San Andreas system can occur here. The 1992 Joshua Tree-Landers-Big Bear earthquake sequence revealed the significance of the fault system that bounds the eastern margin of the range. To the north impressive thrust scarps of the North Frontal fault bound the range but appear to have last ruptured thousands of years ago. Important questions to address on the field trip include (1) can tectonogeomorphic features owing to local block adjustments be distinguished from features owing to broader plate margin interactions, (2) do tectonic structures along the Mojave Desert margin of the range have similar time-space histories as structures along the southeast margin of the range, and (3) what is the evidence for a two-sided uplift history for the San Bernardino Mountains within the broader San Andreas system?

INTRODUCTION

The 'Big Bend' region of the San Andreas fault system provides an archetypal example of a continental transform boundary oriented oblique to the relative plate motion vector (Figure 1). Though dominated by horizontal motion this transform boundary has experienced significant vertical strain and orogenesis resulting from transpression (Matti and Morton, 1993; Weldon et al., 1993; Dibblee, 1982). To better understand mechanisms of crustal deformation along the San Andreas fault system, this field trip will examine the architecture and kinematic history of structures in the San Bernardino Mountains and their margins. The San Bernardino Mountains extend from near field to intermediate distance from the San Andreas fault zone and have risen in the past few Myr (Dibblee, 1975; Meisling and Weldon, 1989; Spotila et al., 1998; and Spotila

In Clifton, H.E., and Ingersoll, R.V., eds., 2010, Geologic excursions in California and Nevada: tectonics, stratigraphy and hydrogeology: Pacific Section, SEPM (Society for Sedimentary Geology) Book 108, p. 273-322.

and Sieh, 2000). This young mountain system and its tectonic margins therefore offer an ideal opportunity to examine long-term transpressive orogenesis associated with the San Andreas fault system.

Complex interaction of intersecting faults is one key aspect of orogenesis in the San Bernardino Mountains. Faults define four distinct crustal-scale blocks within the San Bernardino Mountains (Spotila et al, 1998; 2000): the Big Bear plateau, San Gorgonio Massif, Yucaipa Ridge block, and Morongo block (Figure 2). Thrust fault systems bound the north and south margins of the Big Bear block, as well as the south margin of the Morongo block, and high-angle oblique-slip faults border the San Gorgonio Massif and Yucaipa Ridge blocks. In addition, strike-slip faults of Eastern California Shear Zone intersect thrust faults at the northern edge of the San Bernardino Mountains (Figure 1). Understanding time-space histories of these intersecting fault systems can help distinguish local block adjustments from broader transform plate margin interactions.

The exceptional complexity of the San Andreas fault zone in the region of San Gorgonio Pass also presents a formidable challenge to forecasting the source characteristics of future earthquakes there. Here, a 15 km-wide compressional stepover forms the largest crustal-scale discontinuity in the 1100 km length of the fault and has led to competing models for large San Andreas earthquakes. One scenario envisions a fault system that is continuous through the Pass and capable of generating an ~**M** 7.8 earthquake that ruptures from the Salton Sea to the Mojave Desert (Jones et al., 2008). An alternative model argues that the structural complexity arrests through going ruptures and limits their size to <**M** 7.5 earthquake on either the side of the Pass region (Sykes and Seeber, 1985; Carena et al., 2004; Langenheim et al., 2005).

This three-day field trip will explore sites that illustrate the spatial and temporal Quaternary evolution of the San Bernardino Mountains and their margins (Figure 2). Day 1 focuses on the active tectonics of the San Andreas fault zone and the competing models for large earthquakes summarized above. Day 2 will examine the Quaternary evolution of the Yucaipa Ridge, San Gorgonio, and Big Bear blocks. Day 3 explores the deeply weathered profile atop the Big Bear block and finishes with visits to sites at the intersection of the North Frontal fault system and the Eastern California Shear Zone.

DAY 1

Overview

Distances in miles (and cumulative mileage for the day in parentheses) begin in Garnet, CA (Exit 120, Interstate 10) at the intersection of N. Indian Canyon Dr. and Garnet Ave., located just south of Interstate 10. Stops will explore the active structures of the San Andreas fault zone in the northern Coachella Valley and San Gorgonio Pass including the Garnet Hill fault, the Coachella Valley Banning fault, the San Gorgonio Pass fault system, and the San Bernardino San Andreas fault, and related folds (Figure 3). The main topics for consideration include: (1) along-strike changes in the style and geometry of active faulting and folding, (2) models for slip transfer through the structurally complex San Gorgonio Pass region, and (3) potential sources of large earthquakes.

Directions to Stop 1-1

Drive 0.25 mi south to the west end of Garnet Hill, park in large pullout to the east.

Stop 1-1. Garnet Hill

From the parking area walk to the flank of Garnet Hill, a low hill rises from a broad alluvial plain that fills the northern Coachella Valley (Figure 3). Garnet Hill is a growing fold created by dextral-reverse slip across a left stepover in the Garnet Hill fault. To the northwest, Hugo Hill and East Whitewater Hill are also growing folds at similar stepovers in the fault. To the east and west the Garnet Hill fault transfers slip via folding at compressive stepovers onto the Coachella Valley Banning fault and San Gorgonio Pass fault zone, respectively.

Some of the world's best ventifacts can be viewed at Garnet Hill. Westerly winds funnel through San Gorgonio Pass and focus on Garnet Hill. Here, wind-driven sand from the flood plain of the Whitewater River has sculpted many of the cobbles and boulders. Look for boulders with polished pits, beveled surfaces, and east-west trending grooves. An increasing number of wind turbines in the area are a further testament to the power of the wind here.

Marine fossils have been reported from outcrops of marine strata of the lower Pliocene Imperial Formation in canyons eroded into the south side of Garnet Hill (Matti et al., 1992).

Directions to Stop 1-2

Return to the intersection of N. Indian Canyon Dr. and Garnet Ave. (0.5). Drive 1.5 (2.0) mi north on Indian Canyon Dr. to Dillon Rd., turn left. Drive 3.0 (5.0) mi to Worsely Rd., turn right. Drive 0.75 (5.75) mi to Stop 1-2, park vehicles on the right shoulder of Worsely Rd.

While driving to Stop 1

Indian Canyon Drive crosses the Coachella Valley Banning fault 1.2 mi north of the intersection with Garnet Ave. Here, buildings on both sides of the road are constructed directly on the fault trace. Dillon Rd. crosses a right stepover in the Coachella Valley Banning fault 0.6 – 0.9 mi to the west of Indian Canyon Drive. The north side of the stepover has a south-facing scarp that grows from a height of ~2 m on the east to ~10 m on the west. This scarp occurs at the southern edge of a truncated alluvial fan. The fault trace on the south side of the stepover is barely detectable, but a 1-m-high shutter ridge occurs ~150 m to the south of Dillon Rd. at the east end of the stepover.

Stop 1-2. Coachella Valley Banning fault as a strike-slip fault

Walk about 150 m to the east of the parking area to view some classic geomorphic features of strike-slip faulting, including shutter ridges, a set of parallel fault splays, beheaded streams, and scarps with opposing facing directions (Figure 4). On a clear day Garnet Hill (Stop 1-1) is visible ~5 km to the southeast.

The shutter ridge here is ~750 m long and 200 m wide and is composed of older alluvium (unit Qoa of Figure 4). It consists of an unusually wide zone of faulting with at least four subparallel fault traces striking ~N70°W (small arrows on Figure 4) but the main faulting appears to cluster at the side of the shutter ridge. Scarps face both to the north and to the south and some scarps change facing direction along strike. Antecedent streams cut across the shutter ridge – a large one at Worsely Rd. and a smaller one at the east end of the ridge – and indicate that the uplift rate of the ridge is less than the stream incision rate. Several small scarps can be seen cutting the fill in the gap at Worsely Rd. where recent stream erosion has yet to remove evidence of the most recent earthquake(s).

The eastern end of the shutter ridge impinges on an alluvial fan remnant (Qoa) that forms an elevated terrace to the south of the fault (Figure 4). Numerous beheaded gullies can be viewed on the old fan surface. The terrace level is 7-10 m above the modern alluvial fan surface to the north of the fault (Qal). It is intriguing to consider the whereabouts of the upstream portion of this older fan. One possible correlation is the old alluvial fan surface to the east near Dillon Rd. (see 'while driving to Stop 1-2'). This possible correlation gives ~1.6 and ~2.0 km of dextral slip since the abandonment of this older fan.

The epicenter of the 1986 M_L 5.9 North Palm Springs earthquake is located ~7.5 km to the north of Stop 1-2 (Figure 3). The rupture is interpreted to have occurred along a plane oriented ~N70°W, 45°NE with a first-motion rake of 180°, indicating pure strike-slip faulting (Jones et al., 1986). First motion solutions for aftershocks indicate predominantly oblique motion (dextral reverse). Surface cracks were observed along the trace of the Coachella Valley Banning fault from Devers Hill to Whitewater Canyon. Cracks were also observed in the fault scarp of the Garnet Hill fault at the mouth of Whitewater Canyon (Sharp et al., 1986). Displacements across these cracks were negligible and interpreted to have resulted from ground shaking, not from fault slip at the surface.

Directions to Stop 1-3

Continue 0.4 (6.15) mi north on Worsely Road, turn hard to the left on Painted Hills Rd. Drive 0.25 (6.4) mi to Old Morongo Rd., bear left. Drive 3.25 (9.65) mi bearing generally SW and merge with Whitewater Cutoff. Drive 0.65 (10.3) mi across the Whitewater River to Whitewater Canyon Road, turn right. Drive 1.4 (11.7) mi, turn left onto dirt road (if gate is locked, park and walk to Stop 1.3). Continue 0.1 (11.8) mi to 'T' intersection, turn left. Continue 0.1 (11.9) mi to another 'T' intersection, turn right. Continue 0.4 (12.3) mi to end of road and park.

While driving to Stop 1-3

The drive to Stop 1-3 travels through a valley bounded by the Coachella Valley Banning fault on the north and the Garnet Hill fault to the south. About halfway to Whitewater Canyon, the road passes immediately north of East Whitewater Hill, a hill located at a left stepover of the Garnet Hill fault (Figure 3). Descending into Whitewater Canyon, road cut exposures show a well-developed, orange-weathering soil beneath the upland alluvial fan surface; also note the coarse alluvial gravel that comprises the outcrop beneath the soil. Once across the Whitewater River, the south facing scarp of the Garnet Hill fault is apparent to the north of the road (Matti et al., 1985). Several buildings are constructed at the base of this scarp.

Stop 1-3. Coachella Valley Banning fault as an oblique-slip fault

The view to the east from the parking area reveals thick vegetation upstream from a distinct lineament across Whitewater Canyon (Figures 5). Here the Coachella Valley Banning fault is an aquitard and raises groundwater to shallow levels. An oasis of lush vegetation grows year round on the upstream side of the fault. Vegetation is scarce on the downstream side of the fault where ground water levels drop rapidly in the porous gravel.

The vegetation-covered lineament is aligned with the mouth of the side canyon at Stop 1-3. Walk to the north side of the gulley to view the trace of the fault at the entrance to the canyon (tip of arrow, Figure 5). The fault trace can be followed to the west as it cuts across the side of a steep, south-facing slope. The fault plane is exposed ~0.8 km from Stop 1-3 where it cuts across a tributary of the side canyon (Figure 5). Here the fault strikes E-W and dips N at 45-50°; it contains heavily fractured and faulted granite and gneiss in its hanging wall and Pleistocene alluvial fan gravels of the Cabezon Formation in its footwall. Stops 1-2 and 1-3 show how the Coachella Valley Banning fault changes from a pure-strike slip to an oblique-reverse slip fault in a strike distance of ~5 km.

Directions to Stop 1-4

Return to intersection of Whitewater Canyon Rd. and Whitewater Cutoff, zero the odometer. Turn right (west) and drive 0.15 mi to I-10 onramp, enter Interstate 10. Drive 2.55 (2.7) mi to exit for Haugen Lehman Way. Exit I-10 and follow off ramp for 0.2 mi (2.9) (passing beneath overpass and doubling back), turn left onto Haugen Lehman Way. Drive 0.7 (3.6) mi to intersection with Cottonwood Dr, turn right. Drive 0.8 (4.4) mi to end of pavement. Continue uphill 0.3 (4.7) mi on dirt road to a fork in the road and park. From here hike ~400 m to Stop 1-4, bearing left at fork.

While driving to Stop 1-4

The large hill to the north, known as West Whitewater Hill, exposes fluvial deposits of the Cabezon Formation and is capped by a deep orange-red soil, indicative of ≥100,000 yrs of exposure. The surface is deformed and defines an anticlinal shape. Moderate dips in underlying deposits define this anticlinal warp as well. The deposits appear more deformed than the surface, so the anticline was growing during, as well as after, deposition of the sediments (Yule and Sieh, 2003). Northwest-trending faults cut the deposits and old soil surface (Figure 3).

The composition of Cabezon Formation gravels exposed at West Whitewater Hill indicates a source to the north of the Mission Creek fault, by way of an ancestral Whitewater River (Allen, 1957; Matti et al., 1985, 1992; Matti and Morton, 1993). Paleocurrent indicators in the gravels led Matti et al. (1985, 1992) and Matti and Morton (1993) to propose ~2-3 km of dextral slip across the Coachella Valley Banning fault since the gravels were deposited.

The Garnet Hill fault bounds the southern flank of West Whitewater Hill and has at least two traces, one along the flank of the steep southern slope of the anticline, and another in the young alluvium farther south (Matti et al., 1992, Matti and Morton, 1993, Morton et al., 1987). There is geomorphic evidence that slip on these faults is a combination of dextral and reverse slip, and by the rule of V's, the trace geometry of the northern fault indicates a steep to moderate dip northward.

Stop 1-4. Thrust faults of Cottonwood Canyon

A major change in the style of active faulting occurs at Cottonwood Canyon (Figures 3 and 6). To the east, shutter ridges in gravel as well as channels cut into bedrock show dextral offset along the Coachella Valley Banning fault. Active strike-slip motion on the Coachella Valley Banning fault diminishes toward the west where it appears to end as an active strike-slip fault at Cottonwood Canyon (Yule and Sieh, 2003).

To the west, thrust faults dominate the neotectonic landscape. The active and inactive thrusts include the San Gorgonio Pass thrust and Banning fault systems, respectively. One can explore the evidence for this style of faulting at this stop. Here, several old alluvial surfaces along the mountain front project above neighboring active alluvial fans (Figure 6). For example, ~500 m south of the mountain front a broad active channel separates an old alluvial surface into two remnant terraces. Young alluvium laps onto both remnants except for the western flank of the western remnant that has been eroded. The southeastern edges of both terrace remnants are also eroded, but that erosion occurred in response to uplift of the terraces along a NE-SW-striking, NW-dipping thrust.

Small thrust scarps also occur in young alluvium to the north of the terrace remnants, at the foot of the range. Exposed in the hill above these scarps, granite and gneiss overlie older alluvium along a low-angle, south-dipping contact. This contact in interpreted to be a folded thrust fault (Banning fault?) that is no longer active as slip has stepped southward to the thrusts described above.

A large rotational landslide obscures the geologic relationships of the slopes immediately west of Cottonwood Canyon (Figure 6) (Morton et al., 1987; Yule and Sieh, 2003). The headscarp and lateral margins of this slide are readily apparent and leave no doubt that the feature is of non-tectonic origin. A small sector on the western flank of the slide failed in 1993.

Directions to Stop 1-5a

Return to I-10. Drive west 4.9 mi to the Cabezon exit, zero the odometer. Drive 0.15 mi to stop sign at end of off ramp and turn left onto frontage road. Drive 1.9 (2.05) mi to a roundabout intersection. Continue west on the frontage road for 1.3 mi to Fields Rd, turn right. Drive 0.1 (2.15) mi to entrance gate to Morongo Band of Mission Indians Reservation. (Permission to access tribal lands must be obtained at least one week prior to any field trip from the Tribe's Environmental Office, website: www.morongonation.org and click on "Environmental Department"; phone: 951-849-4697.) Once inside the gate drive 0.4 (2.55) mi north to Sullivan Rd., turn right. Drive 0.25 (2.8) mi to Ramon Rd., turn right. Drive 0.5 (3.3) mi to Martin Road, turn left. Drive 0.75 (4.05) mi to end of pavement and bear left (NE) onto dirt road. Drive 0.65 (4.7) mi to intersection with small dirt road and park.

While driving to Stop 1-5a

Upon approaching the 27-story Casino Morongo and Hotel, look to the north and notice a scarp that cuts at a high angle across the mouth of Millard Canyon. This base of this scarp marks the surface trace of the San Gorgonio Pass thrust. We will visit this feature at Stop 1-5a. The scarp at Millard Canyon continues southwest where it almost intersects Interstate 10 (Figures 3 and 7). Here, cutting through the parking lots behind a large factory-outlet shopping mall, the fault trace bends northwest toward the mountain front along a series of strike-slip tear faults (Yule and Sieh, 2003). After entering the Morongo Reservation, look to the south while driving east on Martin Road and notice that the alluvial surface projects to the roof level of the outlet mall buildings. This surface has been uplifted in the hanging wall of the San Gorgonio Pass fault zone.

Stop 1-5a. Thrust scarp of San Gorgonio Pass fault zone, Millard Canyon

A fluvial terrace riser is evident ~150 m east of the parking area. Climb the riser and walk east to the highest point on the scarp, a height of 12.5 m above the base of the scarp (Figure 7). Walk down the scarp and notice that the slope steepens to a maximum dip at the base of the scarp

This steepening down the slope defines an asymmetric fold and suggests that little, if any, diffusion has occurred across the scarp. Shortening at the surface may be accommodated entirely by folding above a blind thrust. If the thrust has reached the surface here it must have a slip vector of ~S40°E parallel to a small fluvial terrace riser that can be followed from the hanging wall block to the footwall block with no lateral offset (see Figure 6 in Yule and Sieh, 2003).

Walk east from the high scarp and climb down another fluvial terrace riser onto a much younger alluvial surface. Look for a 1.5 m scarp on this lower surface to the east of a dirt road. The west wall of the modern arroyo exposes gravel and sand layers cut by a 24° north-dipping thrust.

Ages of the high and low scarps are poorly constrained. Detrital charcoal from gravel layers beneath the lower surface yield an age of 2850-3600 radiocarbon years (J.C. Tinsley and J.C. Matti in Matti et al., 1992a, p. 26). The poor degree of soil development on the upper surface suggests that it is no older than latest Pleistocene in age. The available age data from these surfaces constrain uplift and north-south shortening each to be >1-2 mm/yr over the past 10,000 yrs or so.

Directions to Stop 1-5b

Drive 0.75 (5.45) mi north to a four-way, dirt intersection and park.

Stop 1-5b. Thrust scarp of Banning fault

Much of the Banning fault in San Gorgonio Pass is inactive. However, a 3-km-long segment of the northern strand is active at Millard Canyon. About 100 m to the north of the parking area, a 5-m-high scarp and a 2.5-m-high scarp occur in older and younger alluvial surfaces. The fluvial terrace riser between these two surfaces appears to show right lateral offset of ~4.5 m (see Figure 8, Yule and Sieh, 2003). Thus the dextral offset across the fault appears to be ~80% greater than the vertical component.

To the east, this active portion of the Banning fault also displaces the late Pleistocene Heights fanglomerate several hundred meters (Figure 7). On the eastern wall of the canyon, the fault trace rises from the canyon floor at a dip of ~45° N and juxtaposes crystalline rocks over the fanglomerate. Farther up the canyon wall the fault flattens to a nearly horizontal dip and overrides the surface of the Heights fanglomerate. Exposures in the canyon wall reveal a buttress unconformity between the fanglomerate and an older eastern wall of the canyon. The base of the buttress unconformity is offset obliquely across the Banning fault with a strike-slip: dip-slip ratio of ~2.5:1, greater than that derived from the younger scar on the valley floor (Yule and Sieh (2003)). Nonetheless, both observations show that strike-slip offset exceeds dip-slip offset on this active section of the Banning fault.

Directions to Stop 1-6a

Return to the intersection of Sullivan Rd. and Fields Rd, turn right, and zero the odometer. Drive 0.5 mi to Morongo Rd., turn left. Drive 0.35 (0.4) mi to Potrero Rd., turn right. Drive 0.65 (1.05) mi to Foothill Rd., continue north through the intersection and a metal gate. Drive 2.75 (3.8) mi along a graded dirt road to a fork in the road at the foot of a small hill. Park and walk to the top of the hill.

While driving to Stop 1-6

Note several up-on-the-north, m-scale steps in Fields Road. A large house is constructed adjacent to the third and largest of these steps. Each step represents a fault trace of the San Gorgonio Pass thrust system. These structures are interpreted as dextral tear faults that connect thrust faults west of Potrero Canyon with those of Millard Canyon (Matti et al., 1985, 1992; Matti and Morton, 1993; Yule and Sieh, 2003).

A terrace riser occurs immediately to the northwest of the intersection of Fields Rd. and Morongo Rd. The upper surface is an isolated erosional remnant that shows an east-west striking scarp, parallel to and north of Morongo Road. Potrero Road crosses this structure and the exposure to the east provides a profile of an asymmetric fold in the hanging wall. This structure is slightly larger, but similar in style, to the scarp observed at Stop 1-5a.

The expression of a scarp along the Gandy Ranch fault (Allen, 1957) occurs ~1 km north of the mouth of Potrero Canyon. The scarp is defined by a subtle warping of the alluvial fan surface here.

Stop 1-6a. Burro Flats overview

Stop 1-6a is located on top of a low east-west ridge (Figure 8). This ridge is underlain by granite and gneiss and capped by a veneer of coarse alluvium, a breccia deposit mapped by Allen (1957). A marshy area occurs at the base of the hill to the north where groundwater ponds against the bedrock. A small up-on-the-south scarp cuts obliquely across the alluvial fan to the north of the marsh. East-trending, down-on-the-south faults occur at the base of the mountains to the north. These east-trending faults comprise the Cox Ranch fault zone, a discontinuous set of dextral, normal-slip faults in the hanging wall of the San Gorgonio Pass thrust (Yule and Sieh, 2003). The Cox Ranch fault zone can be traced east to the Cottonwood and Whitewater Canyon areas where it appears to merge with the Coachella Valley Banning fault. To the west, the San Bernardino San Andreas fault occurs as a series of right-stepping fault segments. The road leading to stop 1-6b runs parallel to the fault. Burro Flats is therefore a fault-bounded, intermontane basin.

On a clear day, this vantage point provides a spectacular view to the southeast of San Jacinto Peak (elev. 3,270 m). The mouth of Potrero Canyon frames the 27-story Casino Morongo Hotel in the footwall of the San Gorgonio Pass thrust system.

Directions to Stop 1-6b.

Drive north 0.35 (4.15) mi to a 'T' intersection, turn left. Drive 1.25 (5.4) mi to fork in road and park.

Stop 1-6b. Burro Flats trench site

The parking area is located at another right-stepover along the San Bernardino San Andreas fault. Walk northwest along the fault trace ~250 m to where the fault branches into two strands at the southeastern edge of another right stepover. Here, in an middle Holocene alluvial fan cut by the fault, a three-dimensional trench excavation was undertaken to explore for buried channels and other features to try and constrain the slip across the fault (Orozco, 2004). A wedge of sand and silt was discovered on both sides of the fault. The wedge tip has 30 ± 15 m of dextral offset and detrital charcoal grains in this layer are ~3,800 yrs old. The slip rate for the San Bernardino San Andreas fault here is therefore constrained at 4-12 mm/yr (Orozco, 2004). A more thorough excavation here may help to better constrain the dextral offset and provide a more precise slip rate.

Farther to the northwest, the fault zone broadens to form a 100-m-wide stepover basin (Figure 9). Here the fault enters a marsh that is partially buried by a recent alluvial fan. Interlayers of peat and alluvium, in combination with active deformation of the stepover basin, make this an ideal paleoseismic site. A series of 10 trenches excavated at this site expose evidence for at least nine paleoearthquakes that span the last 2,000 yrs. The most recent rupture deformed peat layers that contain European-introduced pollen and therefore must post-date ~1750 A.D. This most recent event probably represents the ~M 7.4 1812 earthquake known from sites 50 to 150 km to the northwest. The penultimate event is constrained to have occurred between 1670 and 1730 A.D. and may correlate with a large earthquake ~300 yrs ago that is known from the paleoseismic record in regions both to the northwest and southeast. Five paleoearthquakes at this site correlate in time with ruptures at sites in both the Mojave and Coachella Valley regions. However, the overlap in age data correlations is 50-100 years and cannot rule out the following competing scenarios. One very large (M 7.9) quake may have ruptured a >300 km length of the fault from the Salton Sea to the Mojave Desert. Alternatively two or more large (M 7.4) quakes may have ruptured the same length of the fault over a span of 50 to 100 yrs, perhaps with the structural complexity of San Gorgonio Pass acting as a barrier to thoroughgoing rupture. The former scenario has been adopted over the latter for use in California's annual emergency response and preparedness exercise, initiated in 2008, known as "The Great California ShakeOut" exercise (Jones et al., 2008).

Directions to Stop 1-7

Return to I- 10, zero the odometer. Drive ~2.5 mi west, exit and turn left onto Hargrave St. Drive 0.2 (2.7) mi to W. Lincoln, turn right. Drive 0.5 (3.2) mi to S. San Gorgonio Ave. (Hwy 243), turn left. Drive 7.0 (10.2) mi on Hwy 243 to Twin Pines Rd, turn left and immediately park where convenient on right shoulder. Hike ~0.6 km up a dirt road opposite parking area to the top of the ridge (elevation ~1300 m) for view of structural features expressed in San Gorgonio Pass.

Stop 1-7. Overview of San Gorgonio Pass

On clear days this stop provides a sweeping panoramic view of the tectonic geomorphology of San Gorgonio Pass, Yucaipa Ridge, and the San Gorgonio Massif. From this vantage point one can view most of today's Stops. Stop 1-1 is located nearly 30 km due east of this spot, visible on only the clearest of days. Stops 1-2 and 1-3 lie hidden to the northeast of West Whitewater Hill, recognized by looking toward N75ºE and noticing the hill with the high density of wind turbines at its crest. Cottonwood Canyon and Stop 1-4 can be seen immediately to the west of West Whitewater Hill. Millard Canyon and Stop 1-5 can be seen to the north of Casino Morongo, at a bearing of ~N30ºE. Burro Flats and Stop 1-6 is directly north of this position. Notice the mesa that forms the backdrop to the town of Banning, at a bearing of ~N35-40ºW. This mesa has been uplifted in the hanging wall of the San Gorgonio Pass fault zone; Day 1 Stops demonstrate how the strike-slip dominated Coachella Banning and Garnet Hill faults on the east merge with the oblique thrust-dominated San Gorgonio Pass fault system on the west. One possible explanation involves a gradual northwestward transformation of the San Andreas fault system from a near-vertical strike-slip fault (in the southeastern Coachella Valley) into a shallow-dipping, oblique-reverse fault (along the southern margin of the San Bernardino Mountains) (Yule and Sieh, 2003). In this model the San Bernardino strand forms a sub-vertical tear fault in the hanging wall of the north-dipping thrust system. This structural model of south-under-north, continent-continent collision has important implications for future large earthquakes here.

First, it defines a plausible geometry for future earthquake sources ranging from moderate to large (Table 1, Yule and Sieh, 2003). Second, it provides a basis for modeling of slip and dynamic rupture through the San Gorgonio Pass region. Models that use the thrust geometry yield results that more closely match the geologic slip-rates (e.g. Dair and Cooke, 2009). Third, it provides a starting point for analysis of the partitioning of slip through the region on the various faults, by rotations, and by folding. Models based on geodetic data suggest slow slip rates for the Pass region (e.g., Meade and Hager, 2005) and geologic data support slightly faster slip rates (Orozco, 2004; Yule and Sieh, 2003). Finally, this structural model provides a context in which to understand the paleoseismic data, which could be one of the arbiters of whether or not the several faults move in conjunction or separately.

Before leaving, take in the views of the high peaks here. San Gorgonio Mtn. (3506 m), due north of Burro Flats, is the highest peak in southern California. Little San Gorgonio and Galena Peaks (~2800 m) form the east end Yucaipa Ridge, an elongate ridge to the south of San Gorgonio Mtn. Kitching Peak (~2000 m) is the highest peak to the northeast. These high peaks mark the high points of the structural blocks of the southern San Bernardino Mtns: the San Gorgonio, Yucaipa Ridge, and Morongo blocks, respectively (e.g., Spotila et al., 1998; Spotila and Sieh, 2000; and Spotila et al., 2001). San Jacinto Peak (3302 m) is the second highest peak in southern California, which can be viewed by looking toward ~S70ºE from this spot. It is colliding obliquely with the San Bernardino Mountains. On especially clear days, the Big Bear plateau and Mt. San Antonio (Mt. Baldy) (3069 m) are visible to the northwest. The San Bernardino strand of the San Andreas fault passes obliquely between these two features.

End of Day 1.

DAY 2

Overview

Begin at the intersection of Calimesa Blvd. and Sandalwood Dr. in Calimesa, CA (Exit 88, Interstate 10). Stops will visit structural blocks of the San Bernardino Mountains including the Yucaipa, San Gorgonio, and Big Bear blocks. The primary topics for discussion include: (1) denudation models based on the geomorphology, and thermochronometric and cosmogenic radionuclide data, (2) geomorphologic features of the structural blocks and variations between and within them, and (3) evolution of the San Andreas fault system with time.

Throughout Days 2 and 3 we will see evidence of the uplift/denudation pattern and history that have made the San Bernardino Mountains a classic example of transpressive block uplift (Spotila et al., 1998). We will observe how the intensity of rock uplift and denudation decreases away from the San Andreas fault, which is consistent with models of transpression and is observed along most of the fault throughout California (Figure 10) (Spotila et al., 2007). We will also see what has become a type example for differential "denudational maturity" of crustal blocks (Figure 11) and how geomorphic evolution can be tracked using low-temperature thermochronometry, cross-cutting geomorphic relations and erosion surfaces, and cosmogenic radionuclide dating (Spotila, 2005; Binnie et al., 2008).

Note that while more recent papers by Spotila and Binnie that incorporate thermochronology and cosmochronology form the basis of our quantitative understanding of the uplift history and erosional kinematics of the San Bernardino Mountains, much of the credit for developing the concepts for how the range has evolved goes to earlier work by, e.g., Dibblee (1975), Sadler (1982), and Meisling and Weldon (1989).

Directions to Stop 2-1

Turn right onto Sandalwood Dr. Drive 0.1 mi, bear to the left onto 5th St. Drive 3.7 (3.8) mi, turn right onto Oak Glen Rd. Drive 1.3 (5.1) mi, turn left onto Bryant St. Drive 2.5 (7.6) mi, turn right onto Hwy 38. Drive 2.3 (9.9) mi, turn left onto Warm Springs Truck Rd., turn left onto Morton Ridge Tr. Drive ~1.5 (11.4) mi to gate, park and walk to Morton Peak lookout.

While Driving to Stop 2-1

The west end of San Gorgonio Pass fault crosses Interstate 10 ~0.5 km south of Exit 120 (Figure 3). 5th St. crosses the inactive Banning fault where it is buried by alluvium in Calimesa. The Crafton Hills are located to the northwest of Yucaipa and form the footwall of the Crafton Hills fault zone. Scarps in Holocene alluvium indicate that the Crafton Hills fault is an active structure. The 2005 M 4.9 earthquake with normal left-lateral oblique first motion may have occurred at depth on this fault system. The San Bernardino strand of the San Andreas fault crosses Hwy 38 at the mouth of Mill Creek, ~0.6 mi north of the intersection of Hwy 38 and Bryant St. Hillslopes in Mill Creek canyon here are landslide prone; a relatively recent landslide is apparent on the west wall of the canyon as the road crosses to the west side of Mill Creek. Steep road cuts ~1 mi into the canyon expose Bouma-sequence stratigraphy in the green sandstone and shale member of the Mill Creek Formation (Sadler et al., 1993).

Stop 2-1. Morton Peak Lookout

Here we get an up-close view of crustal slivers that have been uplifted and exhumed along the strands of the San Andreas fault. Consistent with models of transpressive deformation (Teyssier et al., 1995; Fossen and Tikoff, 1998), rock uplift increases towards the fault trace where the obliquity to plate motion exceeds 20° (i.e. pure-shear dominated conditions). Whereas the crustal blocks we will see later to the north are capped by gentle, pre-uplift erosion surfaces and deposits, crustal slivers trapped within the fault zone are extremely rugged and have experienced very rapid exhumation (Spotila et al., 1998). Apatite (U-Th)/He ages from the Yucaipa Ridge block are ~1.5 Ma and indicate a period of very rapid exhumation (~5-7 mm/yr) in the early Quaternary that that has probably continued at a decelerated rate (Spotila et al., 2001 (Figure 12). This rapid uplift either occurred via oblique slip and strain partitioning along the high-angle strands of the San Andreas fault due to its present obliquity to plate motion (i.e. wholesale transpression), or occurred during a finite interval when the block was situated farther to the southeast within the restraining bend of San Gorgonio Pass (i.e. a local geometric complexity) (Figure 13).

Directions to Stop 2-2

Return to Hwy 38, zero the odometer, and turn left. Drive 4.0 mi to Mill Creek Rd, turn right. Drive 4.3 (8.3) mi to Forest Falls picnic area.

Stop 2-2. Forest Falls picnic area

At the foot of the Yucaipa Ridge block, it is easy to see how rapid block uplift has been balanced by rapid erosion. The rugged topography of the block (average long-wavelength slope ~28°, but locally higher) is similar to other locations where steady-state topography has been invoked on the basis of steep average slope near the angle of repose (Figure 14). The hillslope is scarred by numerous avalanche and debris flow chutes, which facilitate the rapid erosion.

Although the maximum exhumation rate for this block occurred ~1.5 Myr ago, long-term exhumation since has been ~1-2 mm/yr (Spotila et al., 2001). Basin-wide erosion rate estimates from cosmogenic radionuclide dating in several drainages on Yucaipa Ridge are reproducible and indicate that erosion rates over the intermediate (i.e. 10^2-10^4 yr) timescale are similarly rapid, averaging 1.5 mm/yr (Binnie et al., 2008) (Figure 15). The similarity of estimates over different timescales suggests that the Yucaipa Ridge block possesses a threshold topography, at which a steady-state has developed, such that exhumation rate is controlled by tectonic uplift rate, rather than short term variations in climate or other factors. As we will see later, the same is not true for the crustal blocks further to the north.

Living at the foot of the Yucaipa Ridge block is dangerous for the community of Forest Falls. This area has witnessed numerous damaging flash floods and debris flows, which recur on average every ~4 years (Morton, 1999). Catastrophic flows are produced by short, intense rainfalls onto the steep drainages of the ridge above, which often exceed the angle of repose and have nearly 3,000 feet of relief. Flows are more damaging where bedrock is highly fractured gneiss and vegetation is sparse. On July 11, 1999, a short-lived afternoon thunderstorm associated with the summer monsoon season dropped 1.5" of rain in the area and resulted in massive, high-velocity debris flows from the Spring Creek, Rock Creek, and Slide Creek drainages that destroyed over 30 homes and resulted in one fatality (Figure 16). A 6-8 ft thick debris flow deposit blocked access via the main road and isolated the community for a day. The maximum observed flow depth was >20 ft, from the base of one debris flow channel to the top of the flow above the overtopped levee. The town itself is built on older bouldery debris flow deposits, and active debris flow channels and levees are widespread in the area.

Directions to Stop 2-3

Return to Hwy 38, zero the odometer, and turn right. Drive 10.8 mi to Jenks Lake Rd. West, turn right. Drive 1.8 (12.6) mi to Jenks Lake, turn left. Drive ~0.1 (12.7) to Jenks Lake parking area.

While Driving to Stop 2-3

Hwy. 38 follows a notch in the western flank of the San Gorgonio block ridge that may represent a wind gap from an ancestral course of the Santa Ana River (Figure 17). While driving through switchbacks, note how the granitic basement is fresher in gullies and weathered when on the outer panels of the hillslope. These outer panels connect with patches of low-relief surface and weathered granite that have been interpreted to be remnants of a widespread weathered erosion surface atop the block that was once connected to the surface on the Big Bear plateau (Figure 17). If time permits, we may stop at an outcrop of weathered monzonite, as well as an outcrop of Santa Ana Sandstone that occurs along Hwy. 38 near Angelus Oaks.

From Hwy. 38 near Angelus Oaks, note the extensive landsliding along the southern perimeter of the Big Bear plateau. This includes the unvegetated landslide scar below Slide Peak, which has built cones of debris near the foot of the Big Bear Creek gorge, as well as the widespread, hummocky deposit of the Seven Pines landslide that occurs to the east of the gorge. This landslide consists of crushed quartz monzonite and overrides the Santa Ana Sandstone (Jacobs, 1982). Keller Peak, the location of Stop 2-5, is visible just to the east of Slide Peak. Also along Hwy. 38 we will cross high angle faults that are the northern boundary faults of the San Gorgonio block. Along Jenks Lake Road near Barton Creek, note evidence of large debris flows with well developed levees that have swept down off of the San Gorgonio block onto Barton Flats.

Stop 2-3. Barton Flats at Jenks Lake

Barton Flats offers views of the impressive San Gorgonio block and southern rim of the Big Bear plateau. These two blocks are respectively considered to be intermediate and immature in terms of their relative stages of denudational maturity (Spotila, 2005) (Figure 11).

The San Gorgonio block contains the highest peak in southern California (Mt. San Gorgonio, 11,504 ft, 3506 m), although the uppermost ridgeline of the block is somewhat rounded and subdued and not the characteristic sharp ridge expected for high peaks of an active mountain range. The southern face of the block is very rugged, but its northern flank is gentler as it plunges northwards towards Barton Flats. Remnant patches of weathered granite are preserved on the block's western and northern ridges, that were once part of the broader erosion surface that existed throughout this area on Mojave-type basement (Figure 17, 18). Remnant deposits of quartzite cobbles derived from a central source atop the Big Bear plateau (Sugarloaf Mtn., 9952') have also been observed on these patches of erosion surface (Sadler and Reeder, 1983). (The erosion surface and gravels will be discussed in more detail at Stops 2-5 and 3-1.) The preservation of these patches of erosion surface imply that the upper portion of the block has not experienced significant syn-tectonic exhumation.

Limited denudation from the top of the San Gorgonio block is consistent with the apatite (U-Th)/He ages from the top of the block, which are old (~55 Ma) and fall into the pool of Laramide-type cooling ages that are found throughout the Southwest. Profiles of the remnant weathered surface and apatite helium age isochrons define the structural uplift pattern of the block as a northward-plunging antiform (Figure 19) (Spotila et al., 1998). The mean long-term incision rate based on the preservation of the weathered surface on this block is 0.27 mm/yr, which is only slightly slower than the mean rate over intermediate timescales based on cosmogenic dating of 0.42 mm/yr (Figure 15) (Binnie et al., 2008). This is consistent with some acceleration of denudation associated with it being a transient, evolving landform. Numerous incipient captures of gentler, easterly trending river profiles by steeper drainages encroaching from the southeast along the eastern flank of the massif are consistent with the idea that this block is a transient landform.

The top of the San Gorgonio block was glaciated in the late Pleistocene (Wisconsin) and is the only mountain in southern California where evidence of multiple phases of glaciation has been confirmed (Sharp et al., 1959). Remnants of moraines have been mapped for seven valley glaciers, with source areas in poorly-developed cirques at 10,300-11,300 ft (3140-3440 m) and terminations as low as 8700 ft (2650 m). Steep slopes limited the thickness of ice to several hundred feet. The largest glacier was near Dry Lake and was almost 3 km long. The morphology of the moraine deposits are uniquely glacial, rather that from rock glaciers or debris flows, and consist of sharp-crested coarse angular debris ridges and end moraines up to 700 ft (213 m) high.

Barton Flats itself, which is the low-lying area between the high San Gorgonio block to the south and the Big Bear plateau to the north, is an intriguing intramontane basin (Sadler and Morton, 1989). This valley has not been produced simply by erosion, but rather has been a low-lying area since the Miocene that has become sandwiched by convergence and uplift on both flanks. The base of the Flats consists of the Santa Ana Sandstone, a 2000 ft thick deposit of finely bedded coarse sand beds and minor conglomerate, interpreted to have formed in a low-relief flood-plain channel system prior to uplift of the San Bernardino Mountains (Sadler, 1993). The sandstone is light colored and arkosic, relatively unconsolidated and incompetent, with locally high (lacustrine?) clay content and is deposited unconformably on weathered granitic basement that may be correlative to the weathered erosion surface present on top of the Big Bear plateau. Clast provenance of the four conglomeratic facies in the formation include lithologies present both to the north (e.g. Saragossa quartzite, Cactus Quartz monzonite) and south (e.g. Baldwin gneiss), and include rocks that were exposed to the south during the Miocene in what is now the San Gabriel Mountains (e.g. Pelona schist). Sadler (1993) proposed that these garnet-bearing Pelona schist clasts were derived from the Sierra Pelona in the North San Gabriel Mountains prior to offset on the Punchbowl fault and later strands of the San Andreas fault, now 120 km away, and prior to uplift of the San Bernardino Mountains. (Pelona schist clasts may be visible in exposures of the sandstone in the outcrop above the parking area at Jenks Lake.) A minimum Pliocene age for the formation is based on a 6.2 Ma cross-cutting basalt intrusion from the eastern part of Barton Flats (Woodburne, 1975; Sadler, 1993). This indicates that Santa Ana Valley is a structural low and that the Big Bear plateau and San Gorgonio block were uplifted and grew up on either side in the Plio-Pleistocene.

Covering the Santa Ana Sandstone in Barton Flats is widespread Quaternary alluvium that is interpreted to have been shed northwards from the San Gorgonio block as fluvio-glacial debris. Uplift and Pleistocene glaciation of the high San Gorgonio massif have produced large volumes of coarse sediment. Clast composition of this alluvium is dominated by the Precambrian (1750 Ma) Baldwin gneiss, which makes up much of the San Gorgonio block. The broad, un-dissected fan shape of Barton Flats is noticeably stepped. Jenks Lake, although artificial, sits in one of the troughs produced by these steps. These steps are likely small landslides within the unconsolidated sediment that resulted from undercutting via 100 m of incision by the Santa Ana River at the fan's northern terminus as well as a low shear strength of clay-rich layers of the underlying Santa Ana Sandstone (Sadler and Morton, 1989). Although Stout (1976) interpreted the entire Flats as one major landslide, Sadler and Morton (1989) concluded smaller scale landslides could explain the stepped morphology and that the Santa Ana River was more likely diverted by the deposition of the fan, rather than a single major landslide.

The Santa Ana basin in Barton Flats is bound on both sides by faults. Minor high-angle faults juxtapose the Flats from the basement of the San Gorgonio block, which are not well constrained, but have been interpreted to have a component of dextral motion (Sadler and Morton, 1989) as well as normal motion as the head-scarp of a major landslide (Stout, 1976). On the north, the Big Bear plateau has overridden the basin via the north-dipping Santa Ana thrust. The Santa Ana Sandstone is locally overridden by basement and exhibits minor folding, although overall it is not pervasively deformed throughout Barton Flats. The overall structure of the basin is a WNW trending syncline, and most of the exposures in Barton Flats are on the southern limb and thus dip moderately to the NNE. Much of the Santa Ana thrust is buried by Quaternary deposits, including well developed fluvial terraces (e.g. Converse Flats), and late Pleistocene scarps occur only locally. Some young scarps occur where the thrust trace has been modified near intersections with northwest-trending strike-slip faults, including the Deer Creek fault, and may represent local reactivation (Jacobs, 1982). These discontinuous dextral faults may represent incipient southward propagation of the Eastern California Shear Zone into the Big Bear plateau (Spotila and Anderson, 2004). Based on similarities to the Squaw Peak thrust system and Waterman Canyon fault to the west (Figure 18), Meisling and Weldon (1989) suggested that the Santa Ana thrust was active mainly in the Miocene. If so, this margin of the Big Bear plateau may have been built shortly after deposition of the Santa Ana Sandstone in the late Miocene. Curiously, the Santa Ana thrust dies out to the east along the plateau's southern escarpment, suggesting it is not the only structure responsible for its uplift. Note also that the trace of the thrust increases in elevation towards the east, indicating that it has been uplifted by another structure that lies beneath it. This structure is thought to be the south-dipping North Frontal thrust system that daylights along the northern escarpment of the plateau (Spotila and Sieh, 2000), as we will see on Day 3.

Although the upper surface of the Big Bear plateau has been little eroded since initiation of uplift of the range at ~2.5 Ma, the southern rim of the plateau is denuding more quickly. The estimate of long-term incision based on the depth of erosion beneath a projection of the weathered surface above the southern escarpment and Santa Ana thrust fault is 0.18 mm/yr (Spotila et al., 2002). In contrast, the intermediate term denudation rate based on cosmogenic dating is 0.67 mm/yr (Binnie et al., 2008) (Figure 15). This implies that denudation has accelerated along the southern flank, consistent with a model of transitional landscape development for a fault block uplift. Rapid denudation of the southern rim is evident in the widespread landslides that occur along it. These include landslides visible from Hwy. 38 at the western end of Barton Flats, as well as deep-seated bedrock landslides composed of crushed quartzite and underlying gneiss that were sourced from Sugarloaf Mountain to the northeast and came as far south as Barton Flats, which are clearly visible from Jenks Lake. More evidence of the preservation of the weathered surface atop the Big Bear plateau and on how denudation rates have varied with time will be discussed at Stops 2-4, 2-5, and 3.1.

Directions to Stop 2-4

Return to Jenks Lake Rd. (12.8 mi), turn left. Drive 3.0 (15.8) mi to Hwy 38, turn right. Drive 8.6 (24.1) mi to Rainbow Lane, turn right and park.

While Driving to Stop 2-4

Hwy. 38 passes below Sugarloaf Mountain, which is composed of the Precambrian-Paleozoic metasedimentary rocks deposited atop the Baldwin gneiss. This section in the San Bernardino Mountains consists of the Saragossa Quartzite (2000 ft thick) overlain by the Furnace Limestone (4000 ft thick); both units form low-grade roof pendants within the Mesozoic batholith that makes up the majority of the range (Dibblee, 1982). The Saragossa Quartzite consists of vitreous, white, hard quartzite that is likely correlative to the late Precambrian and Cambrian Zabriskie, Wood Canyon, Sterling, and Johnnie Formations found in the northeast Mojave Desert, on the basis of *Scolithus* tubes. This body of quartzite at Sugarloaf Mountain is significant because it is thought to be the source of many of the quartzite clasts found throughout the top of the Big Bear plateau to be discussed at Stop 3.1 (Sadler and Reeder, 1983). The Furnace Limestone is generally recrystallized as a dark gray to white marble, which is thought to be correlative to either the Cambrian Carrarra and Kingston Peak Formations or younger (Mississippian) formations on the basis of brachiopod and crinoid fossils. The late Mesozoic batholithic rocks that surround these roof pendants are typical of the central Mojave Desert and are generally leucocratic granitic in composition, such as the Cactus Quartz Monzonite that makes up much of the eastern flank of the Big Bear plateau.

An excellent exposure of the Santa Ana Sandstone and cap of coarse Quaternary gravels occurs by Glass Road just before the Hathaway Bridge. The gravels contain primarily the biotite-rich Baldwin gneiss and were derived from streams and debris flows coming off the San Gorgonio block. The Santa Ana Sandstone is finer grained, moderately-dipping, and contains pebbles and cobbles of Pelona Schist, granitoid, and metavolcanic rocks. If time permits, we may stop at this outcrop. About 0.3 miles before Stop 2-4 (0.2 miles after the 8000' elevation sign) we may pause to view an outcrop of where the Santa Ana thrust displaces Pliocene basalt over the Santa Ana Sandstone.

Stop 2-4. Tertiary basalts atop the weathered granite surface.

The surface of the Big Bear plateau is characterized by an extensive low-relief upper surface with distinct characteristics that indicate a long history of weathering, erosion, and relative geomorphic stability. This was recognized early on by Dibblee (1975), and further explored by Spotila and Sieh (2000). The latter investigated the degree to which the surface represents a structural datum that could be used to quantify the magnitude of erosion and incision into the plateau, as well as to estimate the magnitude and pattern of rock and surface uplift due to motion along the underlying thrust faults. We will examine exposures of the weathered surface at Stop 2-5 and discuss its history and viability as a datum. In addition, the eastern flank of the Big Bear plateau marks an excellent location to examine the geometry of the surface and magnitude of incision into the plateau.

A structure contour diagram of the weathered erosion surface along the plateau is shown in Figure 20. Note that Hwy. 38 offers intermittent views of the surface to the northeast, where the surface has been disrupted by trances vertical offsets along NW-trending strands of the Eastern California shear zone that penetrate the northern rangefront, including the Helendale, Bighorn, and Pipes Canyon faults. The weathered surface is more planar and regular where it tapers down and connects smoothly with the basement surface of the Mojave Desert at the eastern edge of the plateau, as can be seen from the top of Onyx Mountain. Here, the surface is also locally covered by once-continuous Tertiary basalt flows at Pioneertown and Chaparossa Peak that provide a marker for reconstructing its geometry and the magnitude of incision (Figure 18, 21). These alkali-olivine basalts of an unknown source vent consist of 7-9 correlative flows that total 20-60 m thickness, and range in age from 6.9-9.3 Ma (Neville and Chambers, 1982). The basalts locally overlie as much as 100 m of sandstone, which is thought to correlate with either the Santa Ana Sandstone or the Old Woman Sandstone from the northern range front (Sadler, 1993). Beneath the sandstone and basalt, the quartz monzonite basement is deeply weathered, and where subsequent erosion has removed the weathered detritus, the basement outcrops in the characteristic corestone pattern (Figure 21). At Pioneertown, the basalts create flat-topped mesas that were clearly once continuous, although remnant basalts continue west of the Pipes Canyon fault on isolated peaks (e.g. Ruby Mountain, Antelope Creek, Sleepy Creek, Onyx Peak).

Spotila (1999) constructed a structure contour map of the top of the weathered surface beneath these basalts as exposed in local mesas and isolated remnants on peaks and ridges, and found that the resulting surface was nearly planar and gently (5.5°) tilted to the east. The average depth of the underlying erosional topography beneath this smooth projected envelope is ~150 m, suggesting this magnitude of post-eruptive incision into the plateau surface. This implies a long-term average erosion rate since the youngest basalt of ~0.02 mm/yr, although if this incision primarily took place after the ~2.5 Ma initiation of uplift, the rate would be higher (as high as ~0.06 mm/yr). A comparable estimate of long-term post-Miocene incision rate into the weathered surface comes from where it is covered by the Crowder Formation along the western flank of the plateau (Meisling and Weldon, 1989). Locally the rate of incision would be higher as well, such as in the canyon of Deep Creek that drains the northwestern flank of the plateau to join the Mojave River. These on-lapping relationships atop the weathered surface on the plateau, as well as those that occur in the Santa Ana and Old Woman basins to the south and north, provide the best constraints that the weathered erosion surface had developed by the late Miocene and existed prior to the onset of uplift of the plateau.

Directions to Stop 2-5

Continue north on Hwy 38, cross Onyx Summit (elev. 8443') in 1.6 (25.7) mi. Drive 9.0 (34.7) mi, make sharp left turn into Big Bear City. Drive 1.4 (35.9) mi to intersection with Hwy 18, continue west on Hwy 18. Drive 6.2 (42.1) mi downtown Big Bear City. Drive 3.2 (45.3) mi to Big Bear Lake dam. Drive 11.7 (57.0) mi to Keller Peak Rd., turn left. Drive ~5 mi (62.0) mi to Keller Peak. (Note that Butler Peak is an alternative stop for Keller Peak. It provides a much better view of the transient surface south of Big Bear Lake, but is hard to get to because of the poor quality of the fire road leading to the observation tower.)

While Driving to Stop 2-5

West of Boulder Bay along Big Bear Lake, a remarkably flat panel of the weathered surface rises southwards from Hwy. 18 to the southern rim of the plateau near Clark's Summit, spanning 7000-8000 ft elevation. This surface has the classic bouldery morphology, and while it is not readily visible from the road, it is visible from the northern side of the lake, as we will see on Day 3. Although the surface is nearly flat, incipient drainage captures are already underway along it, including Siberia Creek, showing that this is a classic example of a transient landform. Hwy. 18 then crosses over the dam forming Big Bear Lake. The first dam was constructed in 1883, illustrating just how early water resources were a viable economic pursuit in southern California. The modern dam was built in 1912 downstream of the original, and was improved to meet earthquake engineering standards in 1988

Stop 2-5. Keller Peak Lookout

Keller Peak offers a view of a typical panel of the weathered erosion surface of the Big Bear plateau. This panel is tilted slightly to the northeast, and is down-dropped from one of the highest areas of the surface at Butler Peak by a poorly-known fault system (Green Valley fault; Figure 20). The typical planar geometry of the surface is clearly visible, as is its characteristic form. Throughout the plateau, the weathered erosion surface consists of continuous panels of variable size that are separated by a rejuvenated fluvial network. The topography of these panels.

can be locally very flat, but is generally hummocky and may have local hills with a few hundred meters of relief. Across much of the plateau, the preserved surface is covered by regolith from deep weathering. The weathered profile is up to 30-60 m deep (Spotila, 1999), and grades downwards from a red, clay-rich accumulation horizon near the top, through a pervasive C-horizon of primarily grus, to a zone of mixed C-horizon and spheroidal, 1-10 "corestones" of fresh bedrock (Figure 22). These horizons are visible to variable degrees in outcrops along the plateau, but often the surface is manifest as a bouldery armor of corestones and jointed, spheroidal bedrock, where the loose regolith has been removed by erosion. This characteristic saprolite profile has been described across much of the Mojave Desert (Oberlander, 1972) and is comparable to the weathered profiles developed on granitic rock in other locations worldwide (Spotila, 1999). Thermochronology supports the interpretation that the plateau surface has been minimally eroded. Apatite (U-Th)/He ages from the top of the plateau are old (~50-60 Ma), like the top of the San Gorgonio block, and isochrons are roughly co-planar with the geometry of the surface (Figure 18, 19). This reinforces the idea that the relief in this area was gentle for a prolonged period prior to onset of recent uplift.

The Big Bear plateau is a classic example of a disequilibrium landform that is in the process of rapid adjustment to base-level change (i.e. denudationally immature; Figure 11). Much of the drainage network atop the plateau may be inherited from prior to uplift, but is now rejuvenated by incision. An example of this is Deep Creek, which make a deep canyon into the plateau, but is overall a steep, concave fluvial profile with several minor knickpoints (Figure 23). In other areas, drainage capture has clearly taken place. The best example of this is Bear Creek, located east of Keller Peak. This drainage appears to have eroded headward through a former divide to capture a portion of the low-relief drainage atop the plateau. The location of the capture, about which Hwy. 18 cuts, is one of the most rugged areas in the San Bernardino Mountains, and Big Bear Creek is extremely steep with a prominent, large scale knickpoint (Figure 23). Above the knickpoint, the fluvial profile that is now flooded by Big Bear Lake is much more gentle. Spotila et al. (2002) speculate that this gentle network once flowed to the WSW to the valley just north of Keller Peak and connected up with the Deep Creek system.

Additional evidence of disequilibrium comes from the difference between estimates of long-term denudation and the intermediate (10^2-10^4 yr) timescale erosion rate. Spotila and Sieh (2000) estimated conservatively that the total denudation since onset of uplift has been limited to less than 50-100 m where the surface is preserved atop the plateau, suggesting a long-term erosion rate of <0.05 mm/yr. This estimate is consistent with better constrained estimates where the surface is covered by Miocene deposits. Although basin-wide erosion rates atop the plateau based on cosmogenic radionuclide dating are lower than observed elsewhere in the San Bernardino Mountains, the rates average about twice as fast as the long-term rates (i.e. ~0.1 mm/yr) (Binnie et al., 2008). This suggests that rejuvenation (i.e. denudational response to drop in base level that propagates upstream from the periphery of the block towards the center) has increased erosion rates atop the plateau (Binnie et al., 2008). We expect that as time progresses, this erosion rate will increase, the plateau will become more dissected, and eventually all traces of the weathered erosion surface will be lost.

The preservation of the weathered erosion surface atop the Big Bear plateau has proven useful in two key respects. First, by marking a horizon of minimal syn-uplift denudation, the surface has made it possible to estimate the average long-term erosion rate for the upper plateau surface and the northern and southern escarpments. Coupled with thermochronology estimates of long-term denudation for the southern blocks, this enabled Spotila et al. (2002) to produce a model of syn-uplift erosion rate for the entire San Bernardino Mountains (Figure 24). This model formed the basis for an investigation of what controls erosion in the San Bernardino Mountains. Spotila et al. (2002) found that long-term erosion rate correlates with the major parameters that are expected to influence denudation, namely topography (slope), active tectonic structures and rock uplift, precipitation, and rock erodibility, but that the individual role of any given boundary condition could not be isolated. They concluded that the pattern of erosion in the San Bernardino Mountains was best described as "coincident determinism", in which the geomorphic expression and erosion of mountains is controlled by the coincidental spatial arrangement of independent variables that facilitate rapid denudation. Binnie et al. (2010) further examined this issue by comparing denudation rates in individual basins at the intermediate timescale based on 10Be dating to precipitation rates, slope, and other variables. The concluded that only tectonic uplift via fault motion could explain differences in erosion rate for different blocks of the San Bernardino Mountains, although variations in other factors, such as precipitation, were essential for facilitating the erosion of these blocks (e.g. removing sediment from valleys).

The second use of the preserved weathered erosion surface atop the plateau has been to reconstruct the vertical deformation produced by the underlying thrust structures. Given that the surface has experienced minimal (i.e. <50-100 m) erosion since uplift initiated, the current position of the surface, minus the pre-uplift paleotopography, provides an estimate of the rock uplift due to thrusting. (We will discuss more evidence for the nature of the pre-uplift paleotopography of the surface at Stop 3-1.) Spotila and Sieh (2000) used the structure contours of the preserved surface on interfluves to "fill in" areas that have experienced rejuvenated incision in between, and in turn used this reconstruction to document the magnitude of uplift, shortening, and changes in dip of the underlying thrust faults. The magnitude of uplift was estimated by comparing the reconstructed geometry of the surface atop the plateau to a structure contour map of where the basement surface is around the perimeter of the range (based on gravity and wells to determine the thickness of alluvium). The uplift along the Santa Ana thrust (a backthrust) was then subtracted, using a simple relationship for how the total vertical motion observed along its trace would decay with increasing distance into the hanging wall (assuming a linear fault). They then estimated the total shortening at the tip of the North Frontal thrust fault in several cross sections. This shortening was held constant down dip, so that changes in dip were required directly below areas in which the magnitude of uplift increased or decreased relative to the thrust tip. The result were three cross sections of the thrust fault subsurface geometry, showing a convex shape on the east, concave shape in the middle, and linear geometry on the west (Figure 25). This speculative analysis was further constrained by hypocenters of earthquake clusters, including several aftershocks of the Landers (1992) sequence that occurred on the thrust plane and the depth of earthquakes to define the brittle-plastic transition. The result showed a complex thrust shape with an overall cork-screw geometry, and indicated that it is feasible for the North Frontal thrust system to have uplifted most of the plateau and connected smoothly with the San Andreas fault at depth beneath the range. The total magnitude of shortening associated with these thrusts was estimated to be ~6 km.

End of Day 2

DAY 3

Overview

Mileages begin in the town Fawnskin, located at an inlet in Big Bear Lake's northwest shore. Stops will visit exposures of the weathered surface and thrust fault scarps on the northern range front. The primary topics for discussion include: (1) further exploration of the deeply weathered erosion surface and its paleotopography, (2) kinematics, geometry, and paleoseismology of the North Frontal thrust system.

Directions to Stop 3-1

Zero the odometer at the intersection of Rim of the World Rd and Hwy 38. Drive 2.0 (2.0) mi west on Rim of the World Dr, turn right onto Forest Road 3N14, also known as Coxey Rd. Drive 1.5 (3.5) mi to Stop 3-1. Park on the side of road opposite a road cut.

While Driving to Stop 3-1

Note how the plateau become more arid over a very short distance as we move away from the southern rim of the plateau. The range has a sharp orographic precipitation gradient that has facilitated erosion along the southern blocks while inhibiting it via arid conditions in the north (Figure 26).

Stop 3-1. Outcrop of saprolite

This outcrop of saprolite shows some of the typical characteristics of the deeply weathered profile (this is location SP1 of Spotila, 1999). The exposure comprises a typical thin A-horizon, a 1-m-thick B_w-horizon of oxidized clumpy grus with moderate pedogenic accumulation (~8% clay, 5YR5/6, bulk density <1.5 g/cm^3), and a C_{rt}-horizon of mixed angular grus and corestones that retains the original rock structure (Figure 22). Better developed soils are found in other rare locations along the weathered surface, which contain higher degrees of redness (10R3/4; dark reddish brown), clay content (up to 47%), and more extreme mineralogic decay (biotite and plagioclase absent, smeary orthoclase, etched quartz) (Spotila, 1999). The most weathered locations match observations of the weathered surface in brick-red profiles preserved under basalts in the Mojave Desert (Oberlander, 1972). These argillaceous horizons are similar to those observed in weathered granite surfaces in tropical locations, such as Sierra Leone or Brazil (cf. Spotila, 1999). Oberlander (1972) proposed that the weathered surface had developed under a pre-existing climate that was more humid than the present day Mojave Desert. However, deep weathering capable of producing thick profiles is possible under a range of conditions, and actively occurs in all but polar or extremely arid locations (Spotila, 1999). Arenaceous, grus-dominated profiles are readily produced by volume expansion during biotite hydration and the resulting fracture and disaggregation of polymineralic components. Most exposures of weathering atop the plateau could thus have been produced in the modern climate. However, it is the rare argillaceous profiles, as well as the overlapping relationships by Miocene deposits, that argue most strongly that the weathered surface was developed over a long period prior to Pliocene uplift. Based on a comparison of characteristics to many other locations where deep granitic weathering occurs, the surface may have developed at ~0.01 mm/yr, in which case it may have taken several million years to form (Spotila, 1999).

One of the key questions in using the weathered erosion surface as a structural datum is the nature of its pre-uplift paleotopography (Spotila and Sieh, 2000). Many of the patches of preserved surface are remarkably planar, although there were clearly positive relief landforms from non-granitic lithologies, which tend to outcrop at higher elevation than the more weatherable granitic basement. For example, the chemically-resistant metasedimentary quartzites are on average 400 m higher in elevation across the plateau than granitic rocks (Spotila, 1999). This suggests the weathered surface has experienced etchplanation, in which differential weathering produces lithology-controlled topography over a long period of weathering and slow erosion. For this reason, only granitic areas were used in reconstructing the weathered surface (Figure 20).

Another clue for the paleotopography of the surface are the deposits of remnant quartzite cobbles that are preserved across much of the plateau. Sadler and Reeder (1983) identified numerous locations where loose cobbles are preserved, often as a single layer of cobbles, which they interpret to be traces of a veneer of late Cenozoic sediment that once covered the plateau. These cobbles have been recycled and are now common in the modern stream channels that no longer source quartzite bedrock. Based on lithology, size, and roundness, they interpreted these cobbles to have been sourced from near the present Sugarloaf Mountain, which was likely a positive relief landform prior to uplift of the plateau. Based on the size of cobbles, they suggest that the pre-uplift topography of the surface had to have minor relief, so as to distribute clasts radially away from the source. The sedimentary system was likely low-energy, however, and most of the relief could have existed due to the quartzite-cored landforms. Similar quartzite clasts occur in the Old Woman Sandstone along the northern rangefront, Santa Ana Sandstone in the south, and in the Mio-Pliocene Crowder formation in the western part of the plateau. In the eastern part of the plateau, cobble provenance includes clasts derived from the Mojave Desert to the north, suggesting this area was higher than the erosion surface at the time. The lack of Mojave-type clasts in the Santa Ana Sandstone, and lack of San Gabriel-type clasts in the Old Woman Sandstone, further suggest there was minor relief in the central plateau area prior to Pliocene uplift.

Directions to Stop 3-2

Return to Fawnskin and turn left onto Hwy 38 (North Shore Dr). Drive ~7 mi to intersection with Hwy 18. Drive east on Hwy 18 (a total of 8.2 (15.2) mi from Fawnskin) and park in a large pull out on the right on the shore of Baldwin Lake.

While Driving to Stop 3-2

The drive along Hwy. 38 along the northern shore of Big Bear Lake provides excellent views of the flat panel of weathered surface rising south of the lake, as well as Sugarloaf Mountain and the San Gorgonio block beyond. Imagine this valley in the mid 1800s, before the lake was dammed, when an active lumber industry grew to supply the citrus industry in young Los Angeles. The area was known to be "infested" by grizzly bears, thus leading to its name. The first readily accessible route up the plateau from the south was the Waterman Canyon Toll Road, constructed in 1892. Prior to this, the main routes were via Cushenbury Canyon on the north, around Onyx Peak on the east, and up a steep trail from Barton Flats (Robinson, 1989).

Hwy. 38 also skirts around Gold Mountain, which rises to 8235 ft and is held up by metasedimenary rocks. Gold Mountain was the location of one of the larger gold strikes in the San Bernardino Mountains. Gold was first discovered atop the plateau in 1855. Sporadic finds and mini-gold rushes ensued throughout the late 1800s, as first placer and then vein deposits in quartzite ledges were discovered. Gold Mountain was one of the more fortunate finds. The San Francisco tycoon "Lucky" Baldwin invested in a prospect here in 1873 that led to construction of large mills, although none of the deposits played out to expectations. Some of the original mines are still visible from Baldwin Lake, such as the Doble mine, which was active for 35 years and is just below a reddish streak of oxidized soil along quartzite of the northeastern part of Gold Mountain. Active gold mining continued in the range until the 1950s. Robinson (1989) estimated that the total value of gold extracted from the San Bernardino Mountains was ~$20M (a few percent of the total gold from California during this period). Today, the most valuable mineral deposits in the range are the marbles along the north range front, which have been mined for cement production since the 1940s, as we will see at Stop 3-3.

Stop 3-2. Baldwin Lake and the edge of the Big Bear plateau

Baldwin Lake is a natural closed depression, which was likely formed by damming a gentle, pre-uplift valley with alluvium and landslide debris shed northwards from Sugarloaf Mountain, as well as by the bedrock ridges that surround it on all other sides. The lake is shallow, with a maximum interglacial depth of ~4 m, a maximum glacial depth of ~6 m, and a maximum possible depth of 16 m based on the height of the surface separating it from Big Bear Lake. The lake is susceptible to cyclic drought and is thought to be dry around 1/3 of the time under the modern climate regime. A record of deposition during glacial climate conditions from 65-20 Ka shows cyclic changes in sedimentary facies related to oscillations in wetter and dryer conditions (Blazevic et al., 2009). The occurrence of a natural lake at 2040 m elevation is further testament to the transient nature of the Big Bear plateau surface.

From the position of Baldwin Lake, we are also approaching the edge of the more continuous portion of the Big Bear plateau. To the east, the plateau surface becomes more irregular due to the modification by northwest-trending secondary fault strands that penetrate the range and bisect the North Frontal thrust system (NFTS) (Figure 27). The most westerly of these is the Helendale fault, which branches into two strands at the base of Cushenbury Canyon, which penetrate the plateau and create a graben-like valley (Lone Valley). This valley is visible along the drive to Stop 3-3. These faults may merge with the Pipes Canyon fault to the southeast, which clearly offsets the plateau surface as well. Further east, other fault strands modify the trace of the NFTS, including the Old Woman Springs fault, Lenwood fault, and the Bighorn fault. The NFTS has a more youthful neotectonic expression to the west of the Helendale fault, with larger and more numerous scarps in Pleistocene alluvium (Spotila and Anderson, 2004). In contrast, the branch of the NFTS to the east of the intersection has a more subdued expression, with scarps that appear older based on higher degree of soil development and more gentle topography of the escarpment itself.

The fault strands that modify the plateau to the east are strands of the nascent Eastern California shear zone (ECSZ), a broad array of discontinuous dextral faults that are subparallel to the San Andreas. The ECSZ extends ~1000 km from San Gorgonio Pass to the Basin and Range and accommodates ~25% of the relative plate motion between North America and the Pacific plate (Savage et al., 1990; Miller et al., 2001). Individual faults in the shear zone have produced significant earthquakes in the past few decades, such as the 1992 Landers sequence. Slip rates on individual strands are generally ~1 mm/yr or less, and most faults contain paleoseismic evidence of Holocene rupture and recurrence intervals of a few thousand years (Bryan and Rockwell, 1995). The presence of strands of the ECSZ within the eastern Big Bear plateau suggests that convergence and uplift along the eastern branch of the NFTS may have become inactive and been replaced by regional dextral shear. There is also evidence that this may have occurred along the western NFTS as well. Minor dextral faults occur within the western Big Bear plateau, including

Guard Shack

the Deer Creek and Sky High Ranch faults. There have also been numerous M>4 earthquakes with dextral, northwest-trending focal solutions that have occurred over the past few decades throughout the plateau, including conjugate events of the 1992 M6.5 Big Bear sequence (Figure 27). The history of motion on the NFTS is not well constrained, but there is evidence suggesting it has decelerated. The long-term slip rate required for the total relief of the range front (~0.5 mm/yr) is greater than the recent slip-rate estimated based on crude soil chronosequence ages for Pleistocene scarps along the range front (0.05-0.30 mm/yr) (Meisling and Weldon, 1989). We will revisit the issue of activity along the NFTS at Stop 3-3.

Directions to Stop 3-3

Drive 9.2 (25.0) mi on Hwy 18 and descend from the Big Bear plateau. Turn left onto Marble Canyon Rd at the entrance to Mitsubishi Cement Corporation, phone number (760) 248-7373. With permission or an escort, drive 1.0 (26.0) mi to Cushenbury Rd and turn right. Drive 1.3 (27.3) mi to fork in the road and bear right onto an unnamed road. Drive 0.2 (27.5) mi and park on the right at the base of an escarpment along the North Frontal thrust system.

While Driving to Stop 3-3

Rt. 18 follows two major grades down the northern flank of the Big Bear plateau to the Mojave Desert below. The first, Johnston Grade, occurs just east of Baldwin Lake. The road passes through Baldwin gneiss, which has been thrust over metasedimentary strata, including Precambrian quartzite that itself has been thrust over Paleozoic quartzite and limestone (Figure 28). These older thrusts are intruded by Mesozoic quartz monzonite. Johnston Grade drops into an northwest-trending, intramontane valley (Lone Valley) with a rift-like appearance, which has been produced by oblique dextral slip along poorly-known northwest-trending fault strands that project from the Helendale fault north of the North Frontal thrust system. The second drop occurs north of the alluviated Cactus Flat and follows Cushenbury Canyon to the base of the range. This route passes through complex intrusions of the Mesozoic batholith, including the main phase of quartz monzonite. This passes into a thick sequence of the Paleozoic Furnace Creek marble, which has a strong contact aureole at the edge of the Mesozoic intrusion. The limestone becomes increasingly brecciated and recrystallized to the northwest, suggesting the northern flank of the range has a complex history of brittle thrust deformation.

Stop 3-3. North Frontal thrust system

Here we see the complex surface expression of the North Frontal thrust system (NFTS), which has been responsible for the majority of uplift of the Big Bear plateau. The NFTS is 80 km long and consists of a complex trace that is over 1 km wide, made up of multiple overlapping, discontinuous strands that are manifest as scarps and folds in Pleistocene alluvium and older shear zones in bedrock (Figure 27). The alluvial apron shed off of the Big Bear plateau into the Mojave Desert is thick, forming a footwall foredeep that has depressed the original basement surface. The maximum vertical offset along the NFTS is 1.6 km, as constrained by the offset of the weathered surface atop the plateau from the buried basement in the foredeep (Figure 29). The modern piedmont consists of coalescing alluvial fans, or a bajada, that steepens towards the range front due to active tilting and has experienced a complex history of deformation.

Although the penetration of the Big Bear plateau by the ECSZ suggests that the NFTS has become inactive, trenching at this location reveals that at least the western branch of the NFTS has been active in the Holocene (Spotila and Anderson, 2004). The NFTS at Marble Canyon includes a prominent, youthful trace, just 3 km west of the Helendale fault (Figure 30). A sharp, 5-8-m high scarp is clearly visible in late Pleistocene alluvium (Qa3). This scarp has locally been incised and back-filled by younger alluvium (Qa2). Because trenching in an older, higher scarp would not necessarily offer evidence of the most recent rupture (Figure 31), we trenched into a 1.2 m high, diffuse, apparent scarp in loose, unconsolidated, younger alluvium, along upward projection of a prominent south-dipping reflector in a reconnaissance GPR profile (Figure 31). A 20-m long, 3-m deep bulldozer excavation revealed a clear stratigraphy of ~0.5 m thick channel gravels and debris flow deposits, containing marble and granitic clasts (Figure 32). A clear 23° south-dipping thrust plane extended from the base of the trench to within 1 m of the surface. This plane offset two prominent white, matrix-dominated, carbonate paleosols 1.7 m in a nearly pure-thrust sense. A lack of a colluvial wedge or other fault traces suggests that this offset was produced by a single rupture. Minimal soil development of the exposed stratigraphy (no redness, less than stage II calcic (K) horizons) suggested the entire pedogenic history was less than ~20 Ka (M. Eppes, pers. comm.). A bulk radiocarbon age from charcoal fragments in a sand lens near the base of the trench of 11,160 yr BP supports this age estimate, and suggests that the rupture likely occurred in the Holocene and that the western branch of the NFTS is active. Scaling relationships for this amount of coseismic slip suggest a 40-km rupture event that would have produced a M_w7.2 earthquake.

These results indicate that the western branch of the NFTS has been active in the Holocene, and thus that the ECSZ has not completely terminated the convergence and uplift of the Big Bear plateau. Continued activity along the NFTS is consistent with an M5.4 aftershock from the Landers sequence that occurred along the thrust plane (Feigl et al., 1995). Interestingly, a rupture on this segment of the NFTS would also lower the normal stress on the San Andreas fault, thereby bringing it closer to failure, similar to what occurred with the Susitna Glacier fault during the 2002 Denali rupture (Spotila and Anderson, 2004). These results also suggest that the confluence of the Helendale fault and NFTS cannot be simply explained as a cross-cutting relationship (Spotila and Anderson, 2004), which is consistent with the fact that no actual offset of either fault system has been discovered at their alluvium-covered confluence. A simple velocity model shows how ~1 mm/yr slip on the Helendale fault (assumed) and 0.16 mm/yr on the western NFTS (observed in the trench) would result in ~1.1 mm/yr slip on a more northerly-trending, oblique reverse-dextral fault within the hanging wall (Figure 33), assuming the eastern NFTS is inactive. This viable model eliminates the problem of having an unstable quadruple junction between these faults, which could only have been explained by spatially variable or oscillating stress regimes (i.e. polyphase deformation) within the crust. It also suggests that a major strike-slip fault occurs south of the range front, which could perhaps connect with the Pipes Canyon fault and eventually to the San Andreas fault via the sinistral Pinto Mountain fault (Figure 27).

Directions to Stop 3-4

Return to Hwy 18 and zero the odometer. Turn left and drive 1.0 mi (1.0) to a fork in the road. Turn onto the right fork (Camp Rock Rd), drive 2.4 (3.4) mi and turn right onto Bauer Rd. Drive 1.0 (4.4) mi and turn left onto Dallas Rd. Drive 0.3 (4.7) mi and park at Cougar Buttes. Time permitting, one can drive 2.0 miles farther east of the Dallas Rd/Bauer Rd to view the western edge of the Blackhawk landslide.

Stop 3-4. Folded carbonate horizons at Cougar Buttes

The NFTS consists of a wide band of deformation, including folding along blind thrusts and backthrusts that occur north of the range front in the alluvial piedmont. Fold structures appear to become more youthful with increasing distance from the range front. The growth and incision of these folds is evident in this exposure across the Cougar Buttes anticline. Pearce et al. (2004) showed used observations along this fold and others like it along the range front to develop a conceptual model for how ephemeral streams in alluvium respond to tectonic uplift. They showed that streams tend to be a single incised channel, become braided above a fold, incise into the fold axis, preserving terraces, and return to a single channel below the fold. The sensitivity of stream morphology and stream profiles to uplift allowed identification of folding that otherwise had no obvious topographic expression. Ephemeral response is clearly visible as changes downstream through Cougar Buttes anticline. This anticline has a maximum amplitude of 20 m, is ~200 m wide, and is cored by a concave northward-vergent thrust that dips 19-25° (Figure 35). The backlimb of this fold is steeper (20-55°) than the forelimb (2-26°), giving it the false appearance of a backthrust. The fold is capped by a thick, resistant petrocalcic horizon, which may have influenced its growth.

The surface expression of convergent structures in the piedmont is strongly influenced by the erodibility of alluvium, as controlled by the composition of clasts and subsequent soil development. Eppes et al. (2002) noted that soils developed on granitic alluvium consist of easily eroded thick, red argillic horizons, where alluvium containing carbonate clasts develops thick petrocalcic horizons that are highly resistant to erosion. Rock-like, 2-5 m thick stage IV-V K-horizons occur in some of the alluvial surfaces along the range front, where limestone clasts are often 95% of the provenance. Indurated petrocalcic horizons may develop in a short period (50-100 Ka). Eppes et al. (2002) developed a conceptual model for how the differential erodibility of these soils can influence the topographic expression of folds on the foreland. Folds developed in petrocalic horizons form ridges, where as those in granitic alluvium remain masked due to erosion until basement is exposed (Figure 35).

Beneath the coalescing Quaternary alluvial fans of the northern rangefront lies the Old Woman Sandstone. This is an important Tertiary unit because it constrains the timing of uplift of the San Bernardino Mountains. The brown, arkosic sandstone contains local conglomerate with clasts derived from the north in the Mojave Desert, including Sidewinder Volcanic rocks from near Victorville. The fanglomerate that overlies it, however, contains clasts derived from the Big Bear plateau, including a majority of clasts from the Furnace Creek limestone in the central part of the rangefront. Along the range front are large exposures of bedrock thrust over the Old Woman sandstone. Based on the morphology of taxa found in the sandstone, its central facies was deposited during the Late Blancan land mammal period of ~2-3 Ma, suggesting a best guess for the onset of uplift as post 2.5 Ma (May and Repenning, 1982; Sadler, 1990).

If time permits, we may make a quick stop to the east at the Blackhawk landslide. This is a 370 million ton rock avalanche deposit that rode out a long distance along the alluviated valley from a source in fractured Furnace Creek limestone. The deposit consists of brecciated marble that is now almost completely lithified due to pedogenic carbonate deposition, and is thus well preserved from erosion. Shreve (1968) suggested that air rafting was the reason for the slides long run-out. The deposit is older than 17,400 yr old (C-14) shells that were dated from playas atop it (Stout, 1982), but is actually not dated. It could be considerably older than the age of these shells. A second, older landslide occurs in this area as well (the Silver Reef), suggesting this area has a long history of large scale bedrock avalanching.

Directions to Stop 3-5

Return to the intersection of Camp Rock Rd and drive south a mile or so to a suitable place to view the Helendale fault in the near distance.

Stop 3-5. Helendale fault

The Helendale fault can be identified by a vegetation lineament (cottonwood trees and grasses) fed by springs that occur along the fault trace. Where exposed the fault dips NE and probably has some reverse motion. North of the vegetation lineament, the low hills to the southwest of the fault are being uplifted in a compressive left stepover in the fault trace.

The interaction of the ECSZ and NFTS raises important questions about the nature of convergence in the San Bernardino Mountains in general. While it is easy to envision much of the uplift as resulting from transpression directly along the oblique San Andreas fault, such convergence does not occur everywhere that the fault is transpressive, suggesting that local geometric complexities are instead the primary driver of near-field transpressive deformation (Spotila et al., 2007). The restraining bend at San Gorgonio Pass provides an excellent source of local convergence, and is an attractive explanation given how all of the uplifted blocks of the range are so nicely symmetric about it. This raises the question of what caused the restraining bend to begin with. The most likely explanation is that the junction of the ECSZ and San Andreas fault, through a myriad of structures, has resulted in deflection of the trace of the San Andreas at San Gorgonio Pass. The deflection would have been localized at the active sinistral Pinto Mountain fault, which separates two domains of opposite vertical axis rotation to the north and south (Figure 36) (Spotila and Sieh, 2000). If the restraining bend has been responsible for convergent uplift of the entire range over the past few million years, however, the range would have essentially remained fixed relative to the geometric feature, rather than being translated southeastwards along the San Andreas fault (Spotila and Sieh, 2000). The migration of the ECSZ into the Big Bear plateau, however, suggests that there has been minor (i.e. ~30-40 km) southeastward motion of the San Bernardino Mountains with respect to the restraining bend during the 2.5 Myr history of uplift (Figure 36) (Spotila and Anderson, 2004). Slow motion of the range with respect to the restraining bend allowed the convergence necessary to produce uplift, but also caused progressive modification of the convergent structures as more and more of the range entered the field of dextral shear (somewhat analogous to a meat slicer).

ACKNOWLEDGEMENTS

The authors of this field guide would like to acknowledge the work of a team of USGS scientists led by Jonathan Matti and Douglas Morton whose work has contributed immeasurably to our understanding of the geologic evolution of the San Gorgonio Pass region. We also would like to thank Ed Clifton and Ray Ingersoll for helpful edits to this manuscript.

REFERENCES CITED

Allen, C.R., 1957, San Andreas fault zone in San Gorgonio Pass, southern California: Geological Society of America Bulletin, v. 68, p. 315-350.

Anderson, K.B., Spotila, J.A., and Hole, J.A., 2003, Application of geomorphic analysis and ground-penetrating radar to characterization of paleoseismic sites in dynamic alluvial environments: an example from southern California, Tectonophysics, 368, 25-32.

Binnie, S.A., Phillips, W.M., Summerfield, M.A., Fifield, L.K., and Spotila, J.A., 2008, Patterns of denudation through time in the San Bernardino Mountains, California: Implications for early-stage orogenesis, Earth and Planetary Science Letters, 276, 62-72.

Binnie, S.A., Phillips, W.M., Summerfield, M.A., Fifield, L.K., and Spotila, J.A., 2010, Tectonic and climatic controls of denudation rates in mountainous terrain: The San Bernardino Mountains, California, Geomorphology, in press.

Blazevic, M.A., Kirby, M.E., Woods, A.D., Browne, B.L., and Bowman, D.D., 2009, A sedimentary facies model for glacial-age sediments in Baldwin Lake, southern California, Sedimentary Geology, 219, 151-168.

Bryan, K.A., and Rockwell, T.K., 1995, Holocene character of the Helendale fault zone, Lucerne Valley, San Bernardino County, California, GSA Abstr. Program, 27 (5), 7.

Carena, S., Suppe, J., and Kao, H., 2004, Lack of continuity of the San Andreas fault in southern California: Threedimensional fault models and earthquake scenarios: Journal of Geophysical Research, v. 109, no. B4, paper B04313, doi: 10.1029/2003JB002643.

Dair, L., and Cooke, M.L., 2009, San Andreas fault geometry through the San Gorgonio Pass, California, Geology, v. 37, no. 2, p. 119-122.

Dibblee, T.W., 1982, Geology of the San Bernardino Mountains, Southern California, Geology and Mineral Wealth of the California Transverse Ranges, South Coast Geological Society, 149-169.

Dibblee, T.W., 1975, Late Quaternary uplift of the San Bernardino Mountains on the San Andreas and related faults, in San Andreas fault in Southern California, edited by J.C. Crowell, Spec. Rep. Calif. Div. Mines and Geology, 118, 127-135.

Eppes, M.C., McFadden, L.D., Matti, J., Powell, R., 2002, Influence of soil development on the geomorphic evolution of landscapes: An example from the Transverse Ranges of California, Geology, 30, 195-198.

Feigl, K.L., Sergent, A., Jacq, D., 1995, Estimation of an earthquake focal mechanism from a satellite radar interferogram: Application to the December 4, 1992 Landers aftershock, Geophys. Res. Lett., 22, 1037-1040.

Fossen, H., and Tikoff, B., 1998, Extended models of transpression and transtension, and application to tectonic settings, *in*, Holdsworth, R.E., Strachan, R.A., and Dewey, J.F., eds., Continental transpressional and transtensional tectonics, Geological Society of London Special Publication 135, p. 15-33.

Jacobs, S.E., 1982, Geology of a part of the upper Santa Ana River valley, San Bernardino Mountains, San Bernardino County, California, M.S. Thesis, California State University, Los Angeles, 107 pp.

Jones L.M., Bernknopf, R., Cox, D., Goltz, J., Hudnut, K., Mileti, D., Perry, S., Ponti, D., Porter, K., Reichle, M., Seligson, H., Shoaf, K., Treiman, J., and Wein, A., 2008, The ShakeOut Scenario: U.S. Geological Survey Open File Report 2008-1150, California Geological Survey Preliminary Report 25, version 1.0, 312 p.

Jones, L.M., Hutton, K.L., Given, D.D., and Allen, C., 1986, The North Palm Springs, California, earthquake sequence of July 1986, Bulletin of the Seismological Society of America, v. 76, p. 1830-1837.

Langenheim, V.E., Jachens, R.C., Matti, J.C., Hauksson, E., Morton, D.M., and Christensen, A., 2005, Geophysical evidence for wedging in the San Gorgonio Pass structural knot, southern San Andreas fault zone, southern California: Geological Socieity of America Bulletin, v. 117; no. 11/12, p. 1554–1572, doi: 10.1130/B25760.

Matti, J.C., and Morton, D.M., 1993, Paleogeographic evolution of the San Andreas fault in southern California: A reconstruction based on a new cross-fault correlation, *in* Powell, R.E., Weldon, R.E., II, and Matti, J.C., eds., The San Andreas fault system: Displacement, palinspastic reconstruction, and geologic evolution: Geological Society of America Memoir 178, p. 107–159.

Matti, J., Morton, D., and Cox, B., 1992, The San Andreas fault system in the vicinity of the central Transverse Ranges province, southern California, U.S. Geological Survey Open-File Report 92-354, 40 p.

Matti, J.C., Morton, D.M., and Cox, B.F., 1985, Distribution and geologic relations of fault systems in the vicinity of the central Transverse Ranges, southern California: U.S. Geological Survey Open-File Report 85-365, 23 p.

May, S.R., and Reppenning, C.A., 1982, New evidence for the age of the Old Woman sandstone, Mojave Desert, California, in Late Cenozoic Stratigraphy and Structure of the San Bernardino Mountains, Field Trip 6, edited by P.M. Sadler and M.A., Kooser, in Geological Excursions in the Transverse Ranges, Geol. Soc. Amer. Cordilleran Sect. Meet. Guideb., 78, edited b J.D. Cooper, 93-96.

Meade, B.J., and Hager, B.H., 2005, Block models of crustal motion in southern California constrained by GPS measurements: Journal of Geophysical Research, v. 110, p. B03403,doi: 10.1029/2004JB003209

Meisling, K.E., and Weldon, R.J., 1989, Late Cenozoic tectonics of the northwestern San Bernardino Mountains, southern California, Geol. Soc. Amer. Bull, 101, 106-128.

Miller, M., Johnson, D., Dixon, T., and Dokka, R., 2001, Refined kinematics of the Eastern California shear zone rom GPS observations, 1993-1998, J. Geophys. Res., 106, 2245-2263.

Morton D., Matti, J., and Tinsley, J., 1987, Banning fault, Cottonwood Canyon, San Gorgonio Pass, southern California, in Cordilleran Section of the Geological Society of America Centennial Field Guide, ed. M. Hill, p. 191-192.

Morton, D.M., 1999, San Bernardino report: Debris flows at Forest Falls, San Bernardino County, CA, July 11, 1999; USGS Provisional Report.

Neville, S.L., and Chambers, J.M., 1982, Late Miocene alkaline volcanism, northeastern San Bernardino Mountains and adjacent Mojave Desert, in Late Cenozoic Stratigraphy and Structure of the San Bernardino Mountains, Field Trip 6, edited by P.M. Sadler and M.A., Kooser, in Geological Excursions in the Transverse Ranges, Geol. Soc. Amer. Cordilleran Sect. Meet. Guideb., 78, edited b J.D. Cooper, 103-106.

Oberlander, T.M., 1972, Morphogenesis of granitic boulder slopes in the Mojave Desert, California, J. Geology, 80, 1-20.

Orozco, A., 2004, Offset of a mid-Holocene alluvial fan near Banning, CA: Constraints on the slip rate of the San Bernardino strand of the San Andreas fault, California State University Northridge M.S. thesis, 58 p.

Pearce, S.A., Pazzaglia, J.F., and Eppes, M.C., 2004, Ephemeral stream response to growing folds, Geol. Soc. Amer. Bull., 116, 1223-1239.

Robinson, J.W., 1989, The San Bernardino Mountains, Big Santa Anita Historical Society, Arcadia, California.

Sadler, P.M., 1993, The Santa Ana basin of the central San Bernardino Mountains: Evidence of the timing and uplift and strike-slip relative to the San Gabriel Mountains, in The San Andreas Fault System: Displacement, Palinspastic Reconstruction, and Geological Evolution, Edited by R.E. Powell, R.J. Weldon, and J.C. Matti, Mem. Geol. Soc. Amer., 178, 307-322.

Sadler, P.M., 1990, Geological transect of the central San Bernardino Mountains, Southern California, 36-68.

Sadler, P.M., 1982, An introduction to the San Bernardino Mountains as the product of young orogenesis, in J.D. Cooper, Geological Excursions in the Transverse Ranges, Southern California, 57-65.

Sadler, P.M., and Morton, D.M., 1989, Landslides of the uppermost Santa Ana River basin and the adjacent San Bernardino Mountains of southern California, Pub. of the Inland Geol. Surv., 2, 356-386.

Savage, J.C., Lisowski, M., and Prescott, W.H., 1990, An apparent shear zone trending north-northwest across the Mojave Desert into Owens Valley, eastern California, Geophys. Res. Lett., 17, 2113-2116.

Sadler, P.M., and Reeder, W.A., 1983, Upper Cenozoic quartz-bearing gravels of the San Bernardino Mountains, southern California: Recycling and mixing as a result of transpressional uplift, in Tectonics and Sedimentation along the San Andreas Fault, Soc. Econ. Paleo. and Mineral., Los Angeles, 45-57.

Sharp, R.V., Rymer, M.J., and Morton, D.M., 1986, Trace-fractures on the Banning fault created in association with the 1986 North Palm Springs earthquake, Bulletin of the Seismological Society of America, v. 76, p. 1837-1843.

Shreve, R.L., 1968, The Blackhawk landslide, Geol. Soc. Amer. Spec. Paper 108, 47 p.

Spotila, 1999, The neotectonics of the San Bernardino Mountains and adjacent San Andreas fault: A case study of uplift associated with strike-slip fault systems, Ph.D. Thesis, California Institute of Technology, 378 p.

Spotila, J.A., 2005, Applications of low-temperature thermochronometry to quantification of recent exhumation in mountain belts, Reviews in Mineralogy and Geochemistry, 58, 449-466.

Spotila, J.A., and Anderson, K.B., 2004, Fault interaction at the junction of the Transverse Ranges and Eastern California shear zone: A case study of intersecting faults, Tectonophysics, 379, 43-60.

Spotila, J.A., Farley, K.A., and Sieh, K., 1998, Uplift and erosion of the San Bernardino Mountains associated with transpression along the San Andreas fault, California, as constrained by radiogenic helium thermochronometry, Tectonics, 17, 360-378.

Spotila, J.A., Farley, K.A., Yule, J.D., and Reiners, P.W., 2001, Near-field transpressive deformation along the San Andreas fault zone in southern California, based on exhumation constrained by (U-Th)/He dating, J. Geophys. Res., 106, 30,909-30,922.

. Spotila, J.A., House, M.A., Blythe, A.E., Niemi, N.A., and Bank, G.C., 2002, Conrols on the erosion and geomorphic evolution of the San Bernardino and San Gabriel Mountains, southern California, Geol. Soc. Amer. Special Paper, 365, 205-230.

Spotila, J.A., Niemi, N., Brady, R., House, M., and Buscher, J., 2007, Long-term continental deformation associated with transpressive plate motion: The San Andreas fault, Geology, 35, 967-970.

Spotila, J.A., and Sieh, K., 2000, Architecture of transpressional thrust faulting in the San Bernardino Mountains, southern California, from deformation of a deeply weathered surface, Tectonics, 19, 589-615Stout, M.L., 1976, Barton Flats Landslide, in Stout, M.L., Geologic Guide to the San Bernardino Mountains, Southern California, Assoc. of Engineering Geologists, 65-68.

Stout, M.L., 1982, Age and engineering geological observations of the Blackhawk landslide, southern California, in Fife, D.L., and Minch, J.A., eds., Geology and Mineral Wealth of the California Transverse Ranges, South Coast Geological Society, 630-631.

Sykes, L.R., and Seeber, L., 1985, Great earthquakes and great asperities, San Andreas fault, southern California: Geology, v. 13, p. 835–838, doi: 10.1130/0091-7613(1985)132.0.CO;2.

Tessyier, D., Tikoff, B., and Markley, M., 1995, Oblique plate motion and continental tectonics, Geology, v. 23, p. 447-450.

Woodburne, M.O., 1975, Cenozoic stratigraphy of the Transverse Ranges and adjacent areas, southern California, Geological Society of America Special Paper 162, p. 1-91.

Yule, D., 2009, The enigmatic San Gorgonio Pass, Geology, v. 37, p. 191-192.

Yule, D., and Sieh, K., 2003, Complexities of the San Andreas fault near San Gorgonio Pass: Implications for large earthquakes: Journal of Geophysical Research, v. 108, no. B11, ETG 9-1–9-23, doi: 10.1029/2001JB000451.

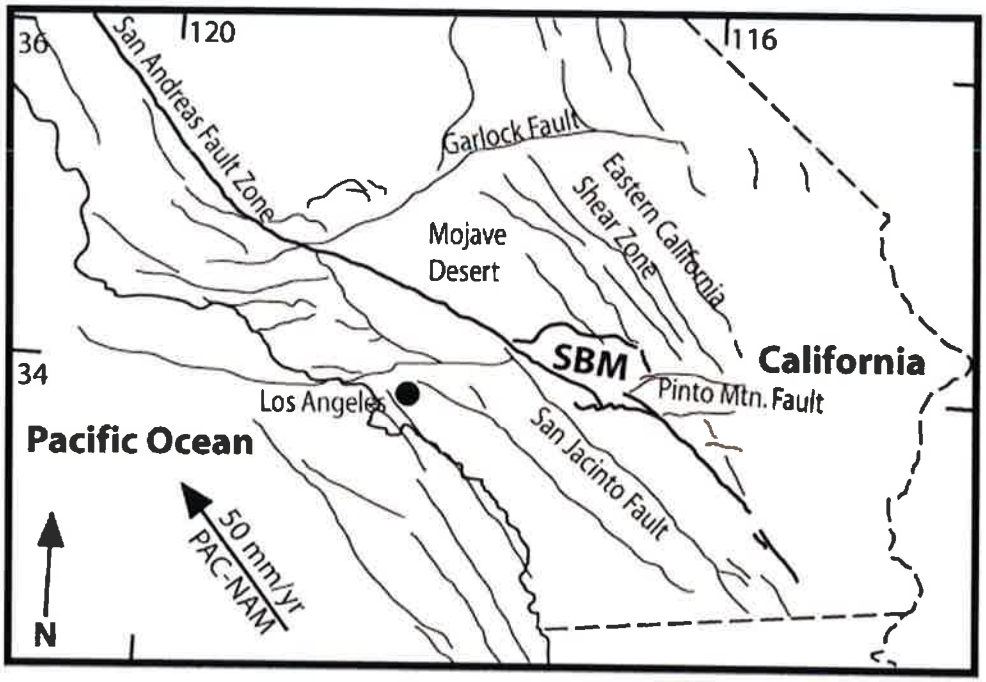

Figure 1. Simplified tectonic map of southern California. The location of the San Bernardino Mountains (SBM) is shown, along with major faults. The vector of Pacific-North American plate motion is also illustrated (DeMets, 1995).

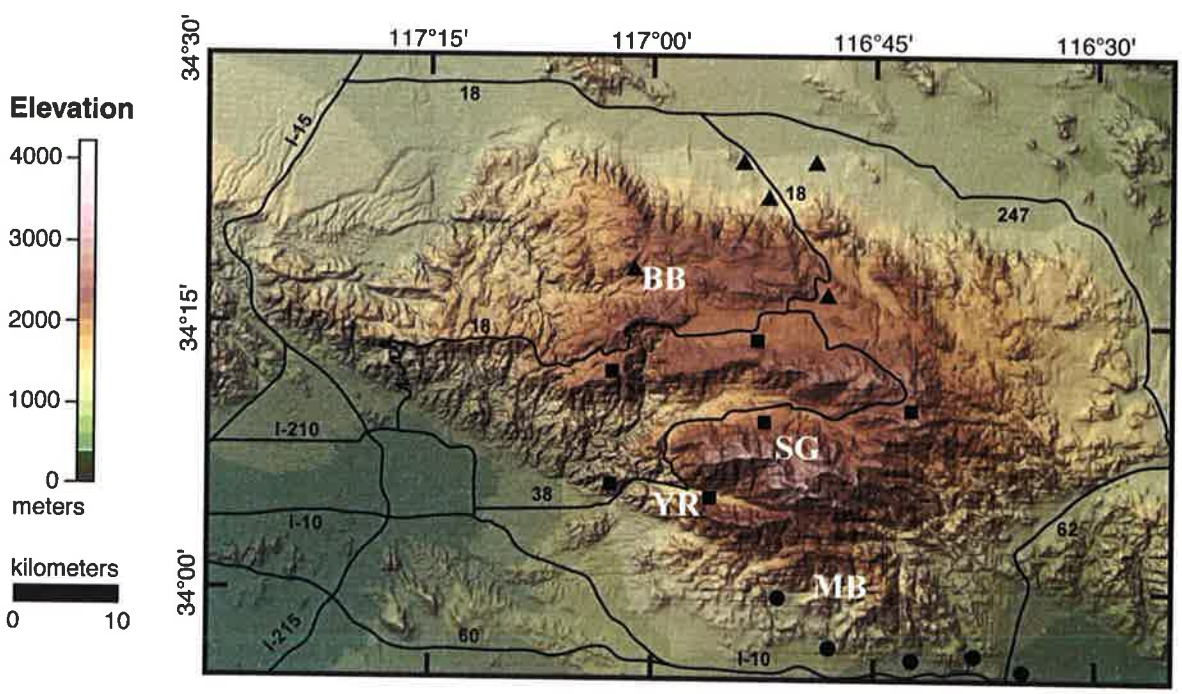

Figure 2. Modified Figure 2 of Spotila et al. (2002). Digital elevation model of the San Bernardino Mountains with Interstate and State Highways superposed. Field trip stops are solid circles (Day 1), squares (Day 2), and triangles (Day 3). BB – Big Bear plateau, MB – Morongo block, SG – San Gorgonio Massif, YR – Yucaipa Ridge block. The shaded relief map is color-coded for elevation and based on 90 m resolution U.S. Geological Survey digital topography (color code based on "newrelief.aml" by Jeff Nighbert, B.L.M., Oregon).

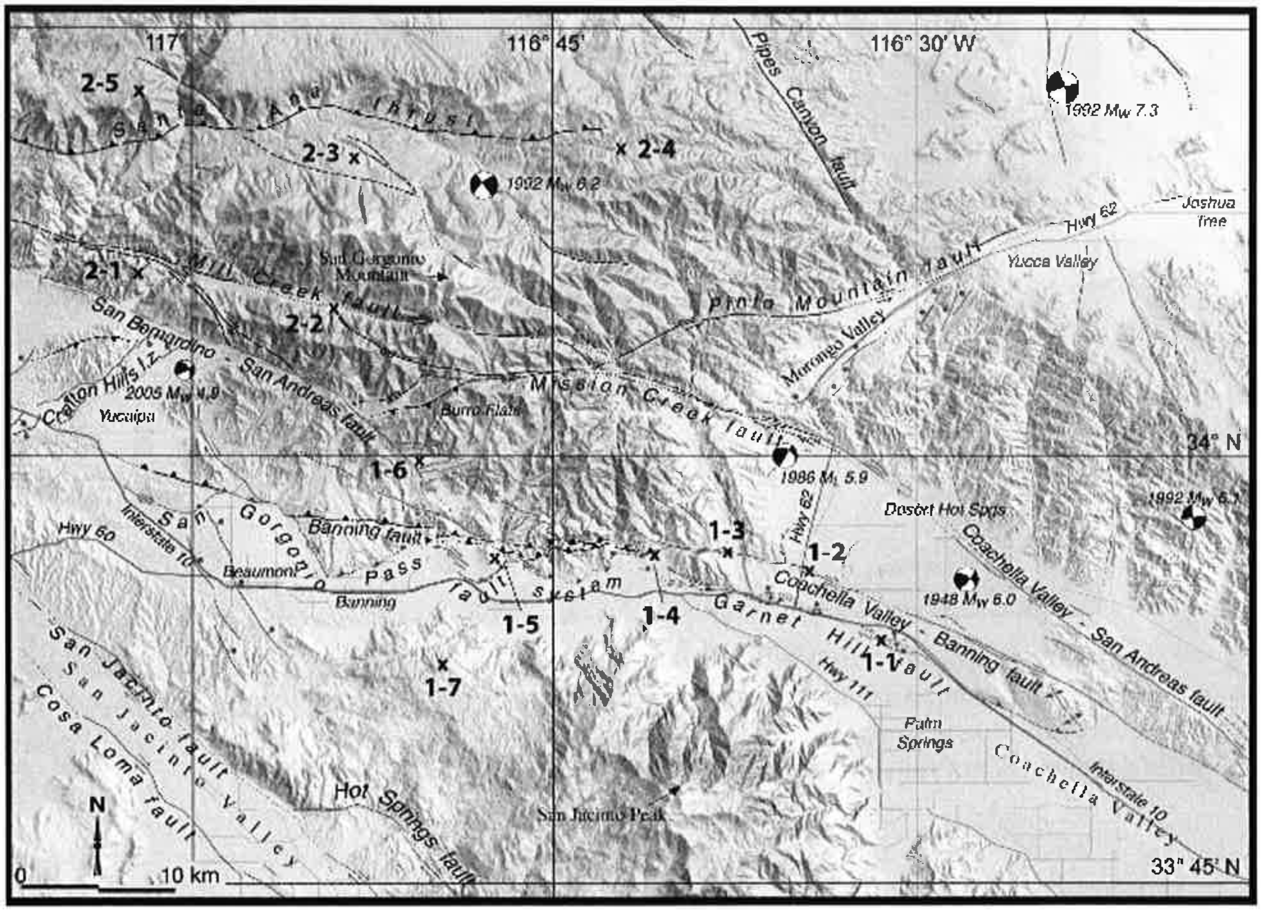

Figure 3. Modified Figure 1 of Yule (2009) with locations of field trip stops for Days 1 and 2. Shaded-relief topographic map of San Gorgonio Pass (SGP) region shows traces of active faults in red, inactive faults in black. Mapping from Allen (1957), Matti et al. (1985), and Yule and Sieh (2003). First-motion diagrams show epicenters of moderate earthquakes to strike the region since 1948

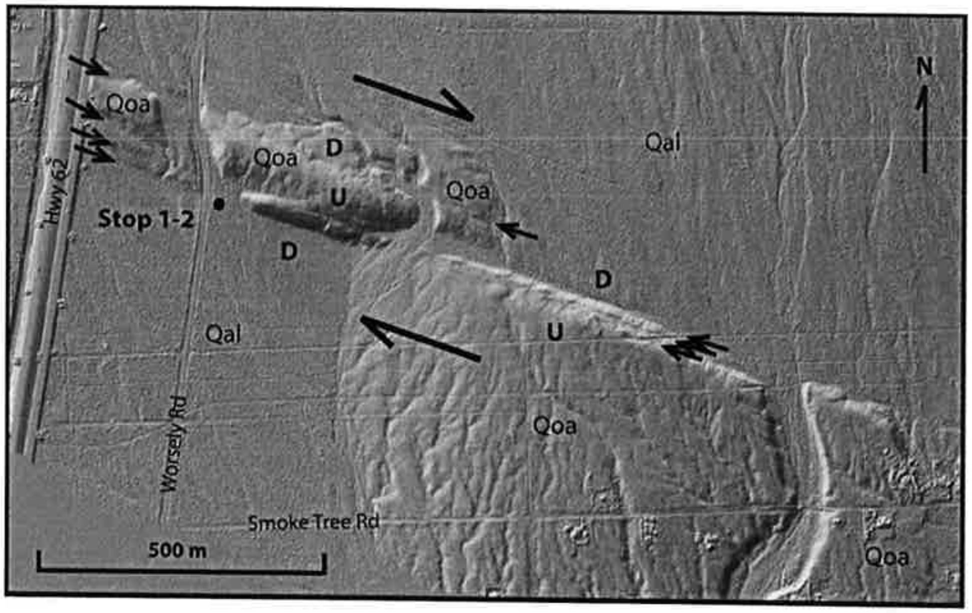

Figure 4. Shutter ridge and truncated alluvial fan along Coachella Valley Banning fault. Image from B4 Project LiDAR Hillshades, Google Earth Topography (http://opentopography.org/). Qal = modern alluvial fan surface; Qoa = old alluvium. Arrows point to four distinct splays. Worsely Rd. follows antecedent drainage that crosses the shutter ridge.

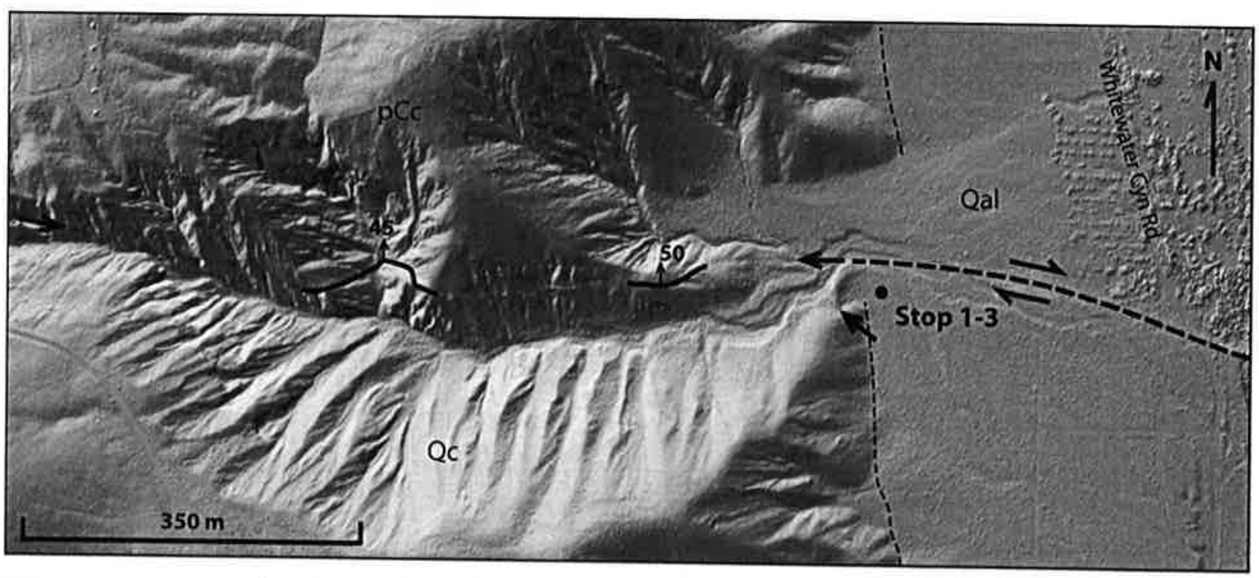

Figure 5. Trace of the Coachella Valley Banning fault at Whitewater Canyon. Image from B4 Project LiDAR Hillshades, Google Earth Topography (http://opentopography.org/). Qal = modern alluvium, Qc = Cabezon Formation, pCc = Precambrian to Cretaceous igneous and metamorphic complex. A vegetation lineament marks the fault trace on the east. Arrows point to fault trace cutting across south-facing slope. Fault dips 45-50° N. A southern splay(?) of the fault may occur to the SW of Stop 1-3; see the arrow tip pointing to scarp-like feature separating crushed granite and gneiss (pCc) from Cabezon Formation gravels (Qc). North-south dashed lines show possible dextral offset of the west side of Whitewater Canyon.

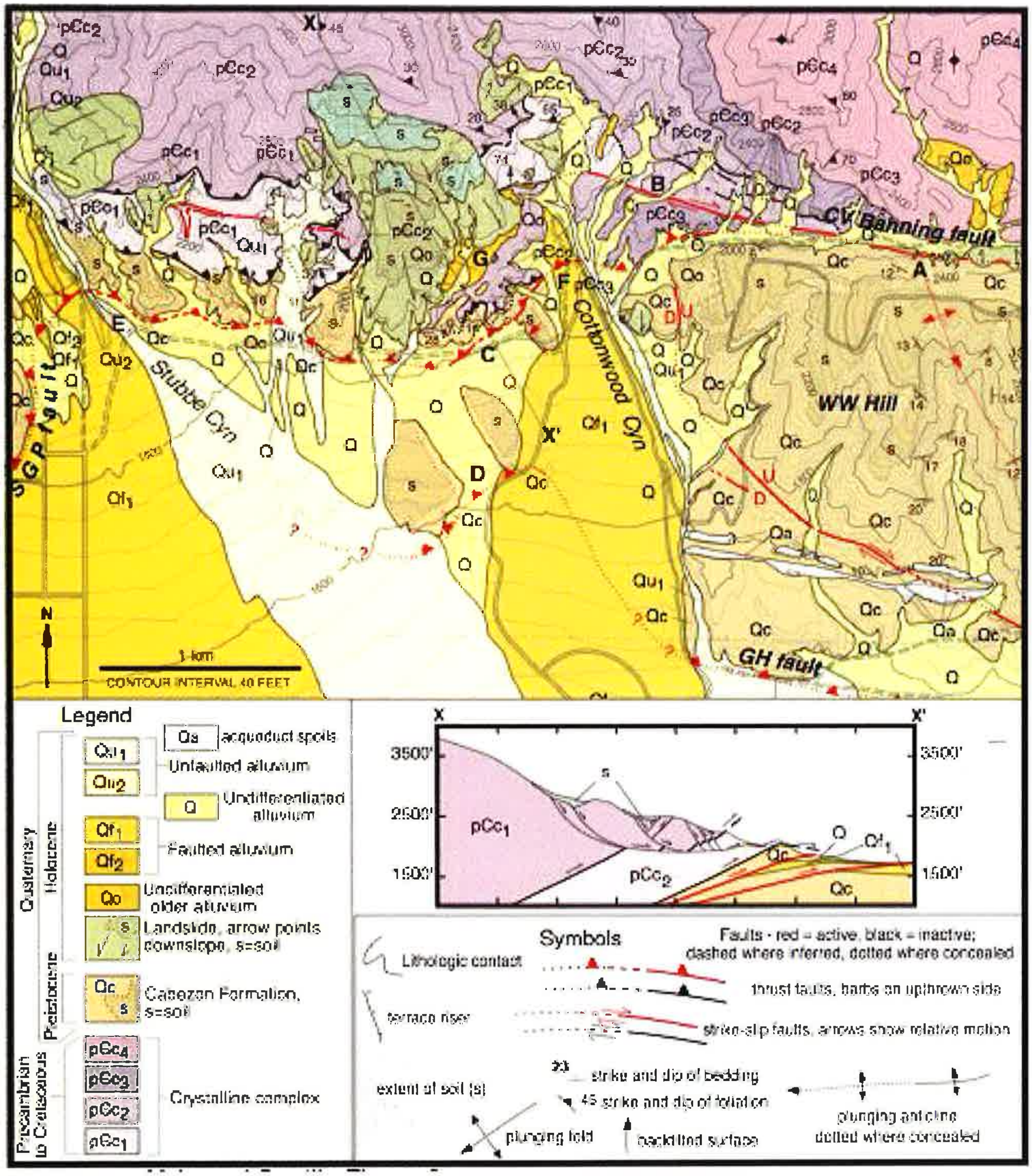

Figure 6. Geologic map and cross section of the Cottonwood Canyon area (combined Figures 11 and 12 from Yule and Sieh (2003), geologic mapping modified from Matti et al., 1992a; Sieh and Matti, 1992; Matti and Morton, 1993; Morton et al., 1987; R. Wolf, unpublished mapping). Stop 1-4 is at 'C', located at the foot of the range. Here, of predominantly right-lateral faults (east of the canyon) merge with predominantly reverse-slip active faults (west of the canyon). Letters A-G refer to geologic features described in text of Yule and Sieh (2003).

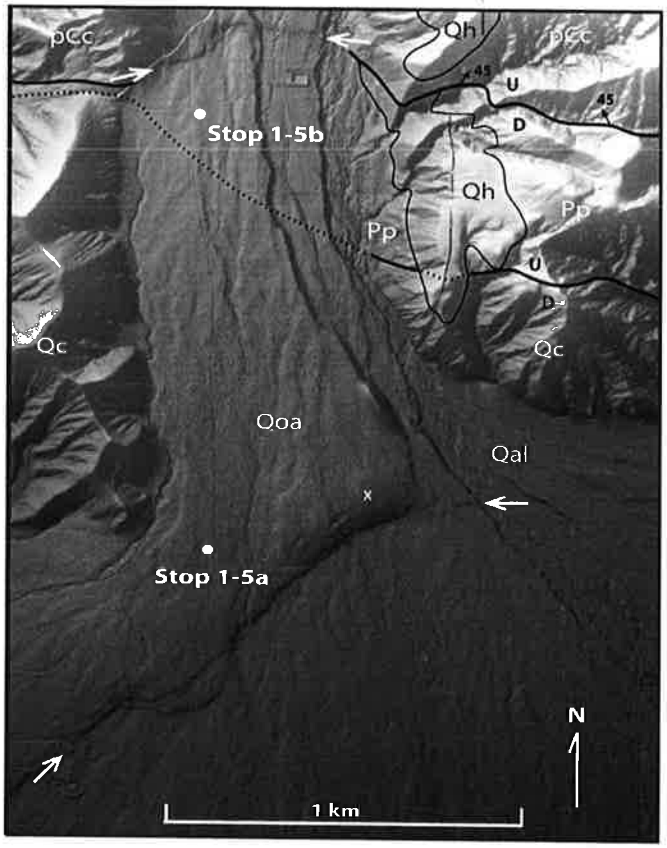

Figure 7. Active and inactive fault traces in Millard Canyon. Image from B4 Project LiDAR Hillshades, Google Earth Topography (http://opentopography.org/).
Qal = modern alluvium, Qoa = old alluvium, Qc = Cabezon Formation, Qh = Heights fangolomerate, Pp = Painted Hill Formation, pCc = Precambrian to Cretaceous igneous and metamorphic complex. White arrows point to fault scarps cutting Qoa. Southern scarp = San Gorgonio Pass fault zone; 'x' locates maximum scarp height. Northern scarp = active segment of Banning fault. Inactive segment of Banning fault separates Pp from Qc and is buried by Qh and Qoa.

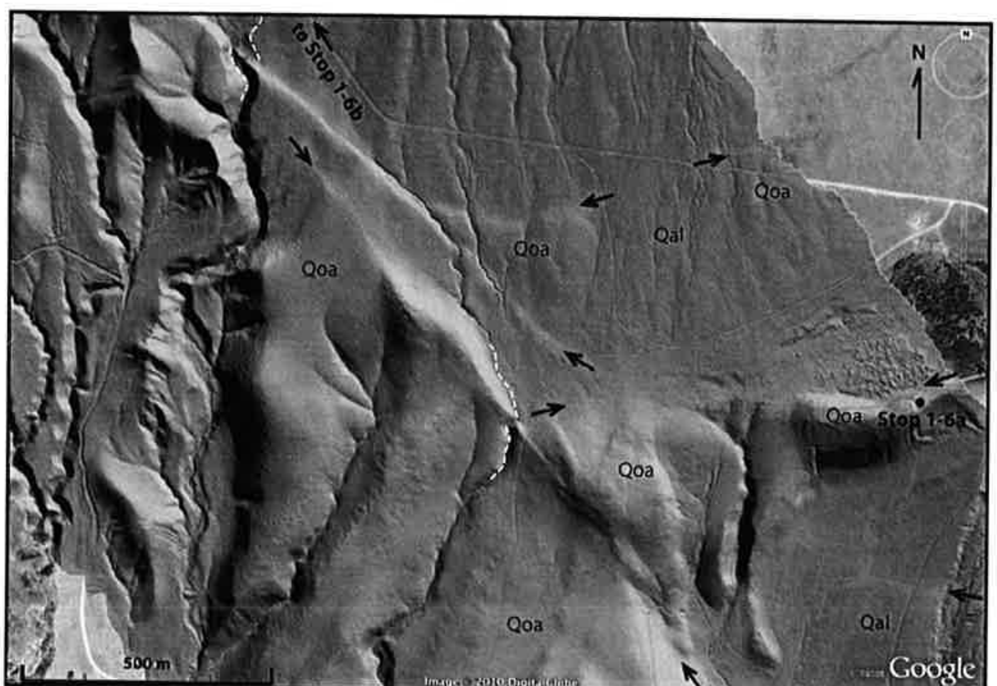

Figure 8. Geomorphic expression of active faults at Burro Flats. Image from B4 Project LiDAR Hillshades, Google Earth Topography (http://opentopography.org/). Qal = modern alluvium, Qoa = old alluvium. Arrow locate fault traces, up on the south and southwest. Dashed white lines locate streams with possible dextral offsets across the San Bernardino San Andreas fault.

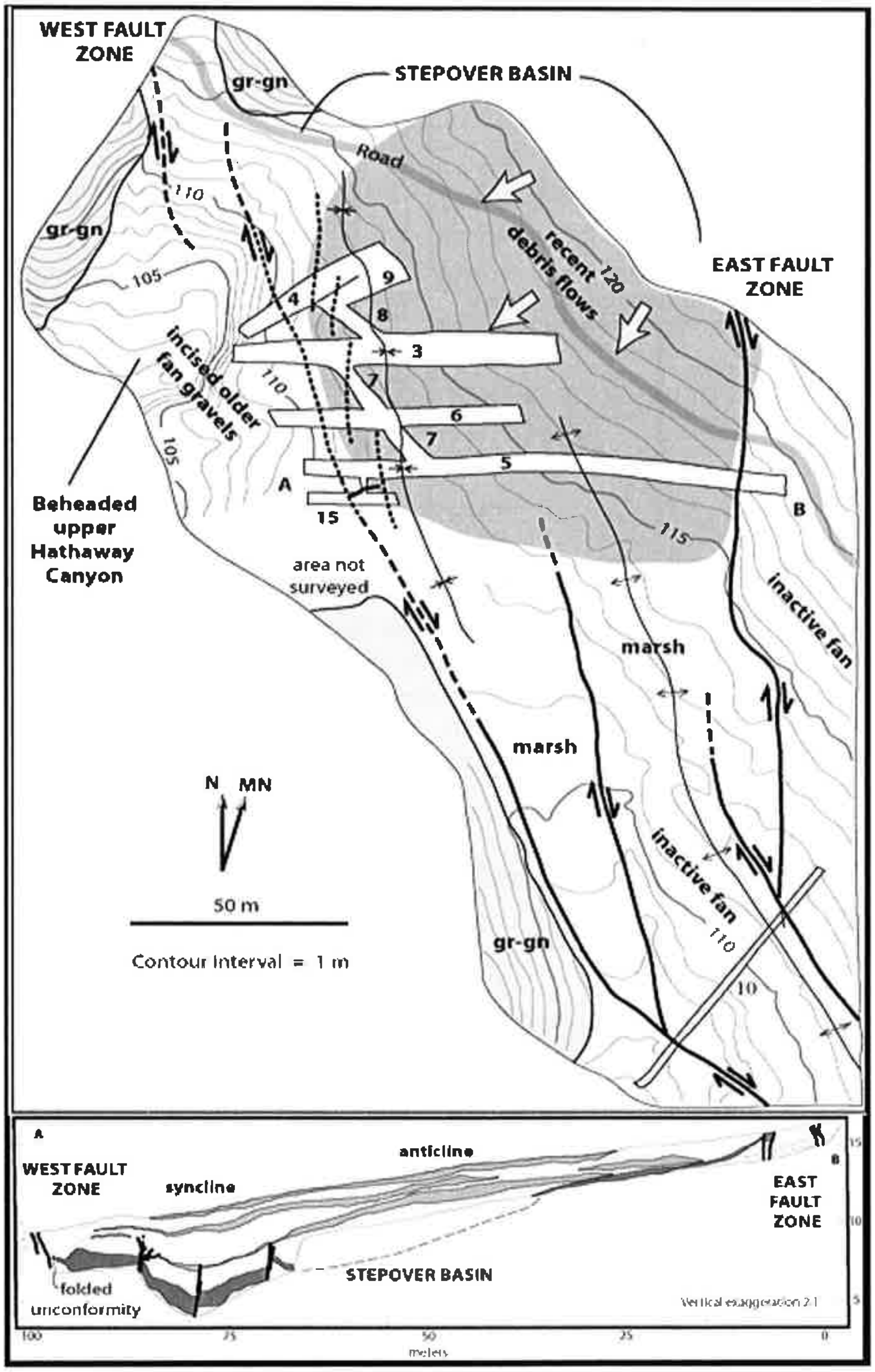

Figure 9. Geologic map and cross section of the Burro Flats paleoseismic trench site, located at a right stepover in the San Bernardino San Andreas fault. Trenches are numbered 1-10 and 15. Cross section is along Trench 5 and shows faults and growth strata (dark gray = thick peat layer at base of Trench 5, light gray = prominent debris flow units). gr-gn = granite and gneiss complex.

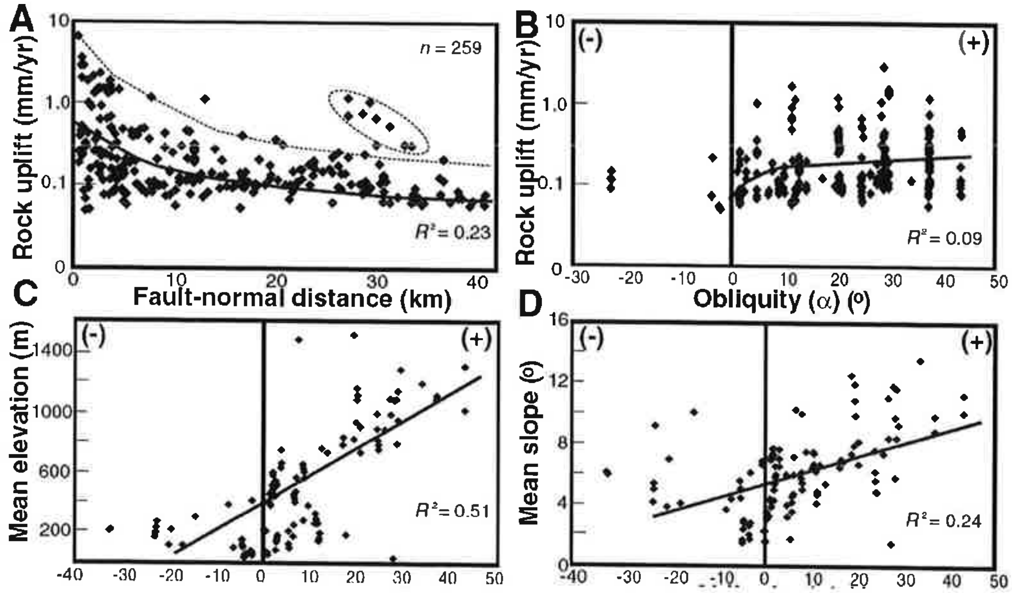

Figure 10. Variation in uplift with distance from the San Andreas fault and degree of plate motion obliquity to the fault trace (α) throughout California (Spotila et al., 2007). A) Variation in uplift with distance from the fault. Note how uplift increases towards the fault, but is somewhat heterogeneous. B, C, and D show how uplift, mean elevation, and mean slope increase with increasing degree of transpressive obliquity between the San Andreas fault and the direction of plate motion.

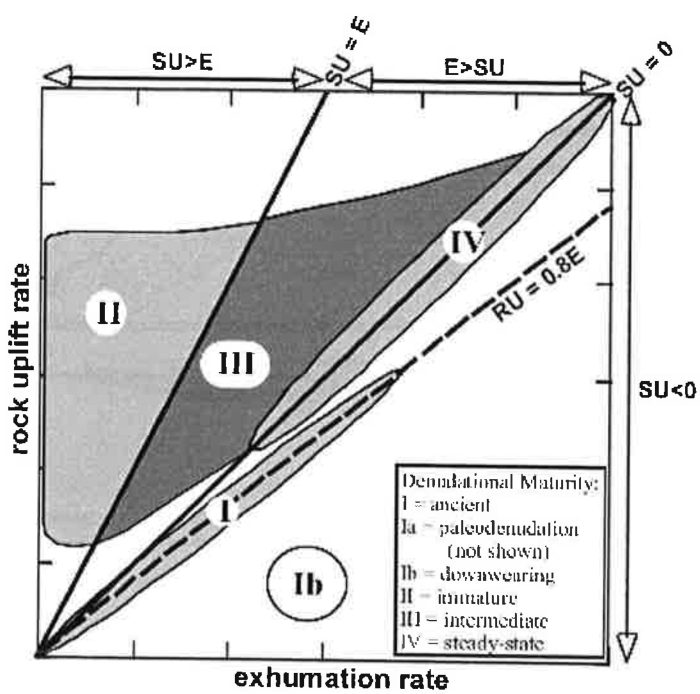

Figure 11. Conceptual model of "denudational maturity", based in part on the evolution of the San Bernardino Mountains (Spotila, 2005). Cases shown are for an ancient, downwearing orogen (I), an immature orogen analogous to the state of development of the Big Bear plateau (II), an intermediate stage akin to the San Gorgonio block (III), and the case of steady-state topography represented by Yucaip Ridge block (IV). Note how the balance of exhumation rate (E) vs. surface uplift rate (SU) vary through the cycle, where rock uplift = exhumation plus surface uplift.

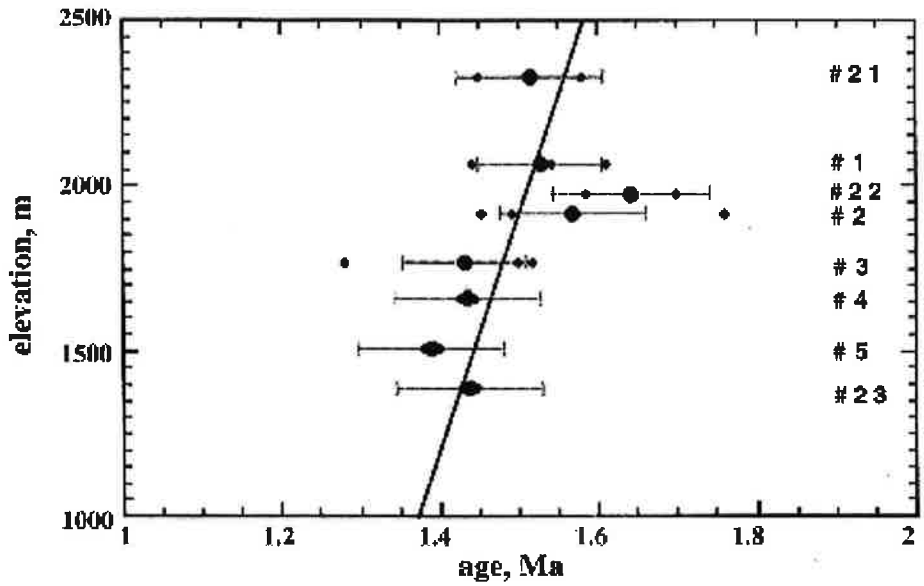

Figure 12. Apatite (U-Th)/He ages along a vertical transect on the Yucaipa Ridge block (Spotila et al., 2001). The age-elevation gradient, as well as a thermal model, indicate that a rapid period of exhumation at 5-7 mm/yr occurred from 1.8 to 1.5 Ma

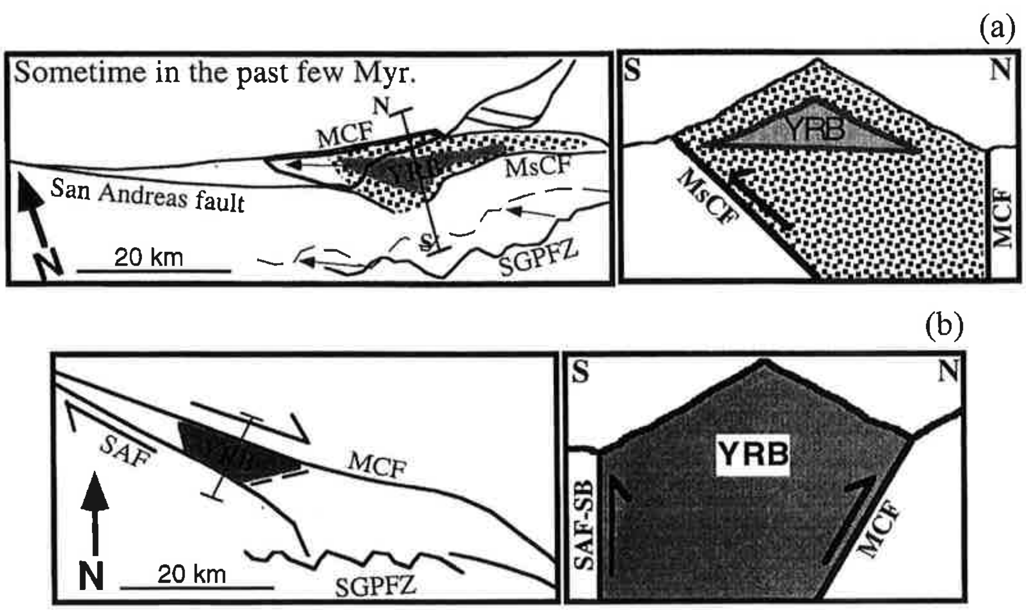

Figure 13. Two possible models for the rapid denudation and uplift of the Yucaipa Ridge block. In a), the rock uplift is interpreted to be due to convergence due to the restraining bend in San Gorgonio Pass, prior to ~10 km of right-slip along the Mill Creek fault. Subsequent to the rapid rock uplift, the block is then translated laterally to its present position. In b), the rock uplift is interpreted to have occurred in its present position due to the regional obliquity of the San Andreas fault.

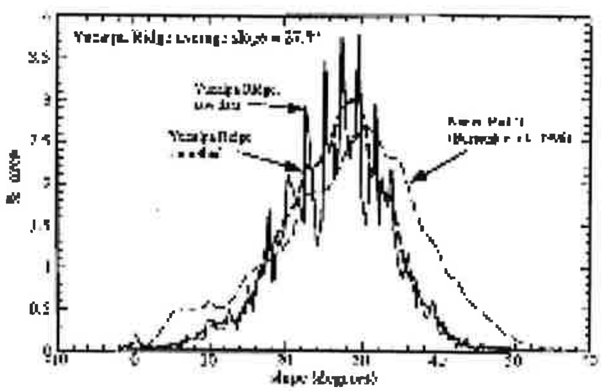

Figure 14. Google-Earth generated image of Yucaipa Ridge, looking south with no vertical exaggeration. Note prominent debris flow chutes and the precarious community of Forest Falls. Plot to the left shows slope distribution of the ridge in comparison to the Nanga Parbat area of the NW Himalaya, where a steady-state topography has been interpreted (Spotila et al., 2001).

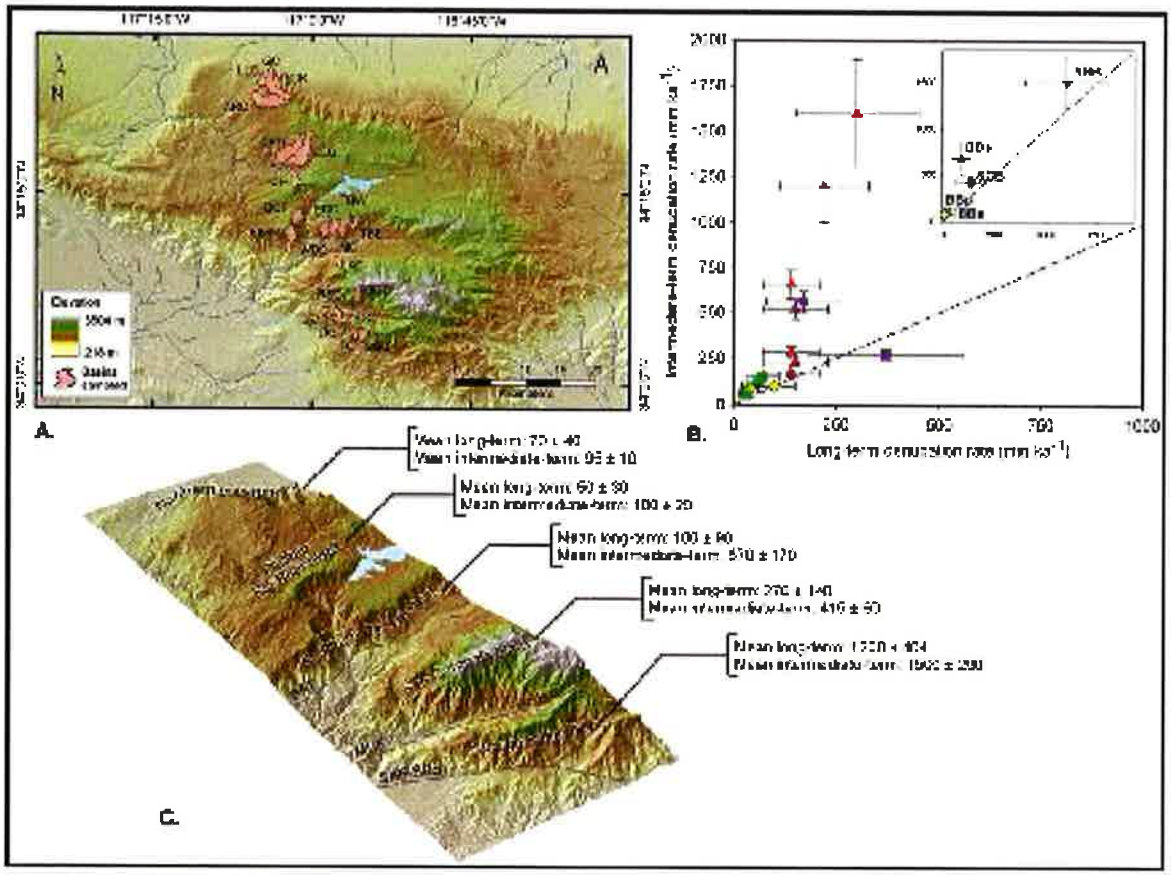

Figure 15. Basin-wide erosion rates based on cosmogenic dating in the San Bernardino Mountains (Binnie et al., 2008). A) Location of basins sampled for ^{10}Be analysis. B) Denudation rates over long-term (10^6 years, based on (U-Th)/He dating and geomorphic markers) versus intermediate term (10^2-10^4 years) based on cosmogenic dating. Note how most blocks, including the Yucaipa Ridge block (YRB), are consistent between timescales on average (inset), but in some cases intermediate-term rates have accelerated relative to the long-term average (e.g. Big Bear plateau: BB). C) Summary comparison of mean long-term and

Figure 16. View up Spring Creek debris flow channel coming off of Yucaipa Ridge following the July, 1999, flood event (from Morton, 1999

Figure 17. Google-Earth image of the Angelus Oaks area, view to the south across the San Gorgonio block. Red polygons are interpreted patches of remnant erosion surface atop the massif, suggesting the top of the block has experienced minimal denudation, which is consistent with thermochronometry. Panels of weathered granite are visible along road cuts on Hwy. 38 (white band) in the area of Angelus Oaks. The low region of Angelus Oaks may be a wind gap that has been uplifted by continued growth of the San Gorgonio block. The modern Santa Ana River drains along the base, joining Big Bear Creek at the blue circle and exiting southwards from the range. Hummocky area near the base of the image is the edge of the Seven Pines landslide.

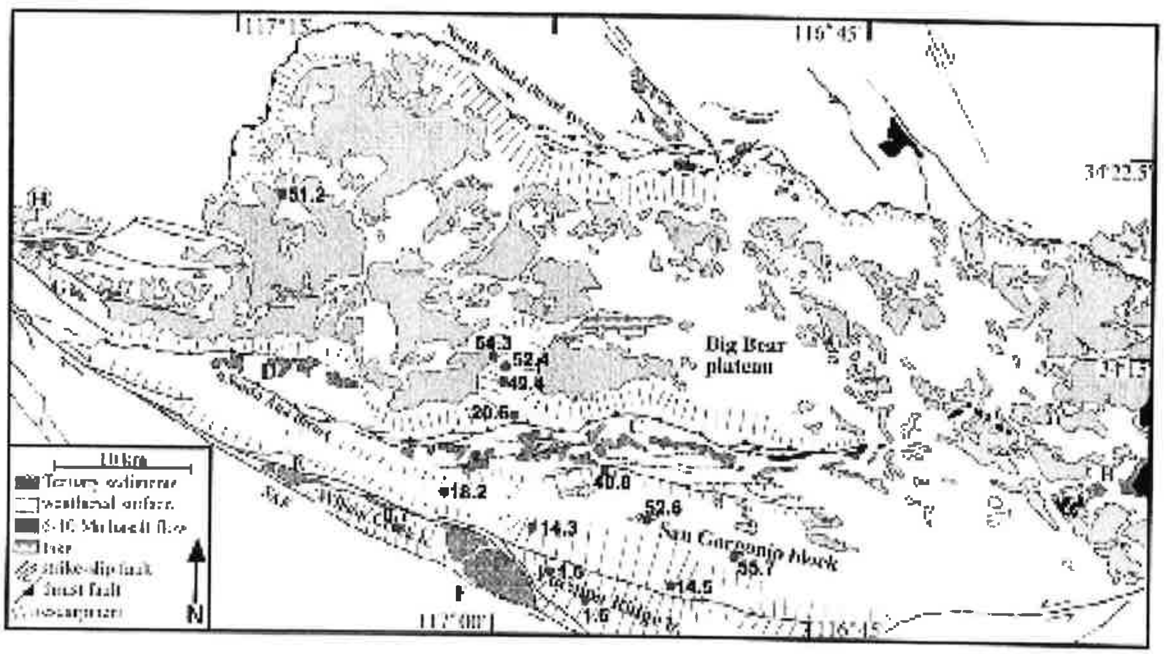

Figure 18. Distribution of the remnant patches of weathered erosion surface (gray) in the various blocks of the San Bernardino Mountains, including the locations where Tertiary deposits overlie it (Spotila and Sieh, 2000). Apatite (U-Th)/He ages (Ma) are also shown from Spotila et al. (1998), but note that the additional ages from the Yucaipa Ridge block from Spotila et al. (2001) are not shown.

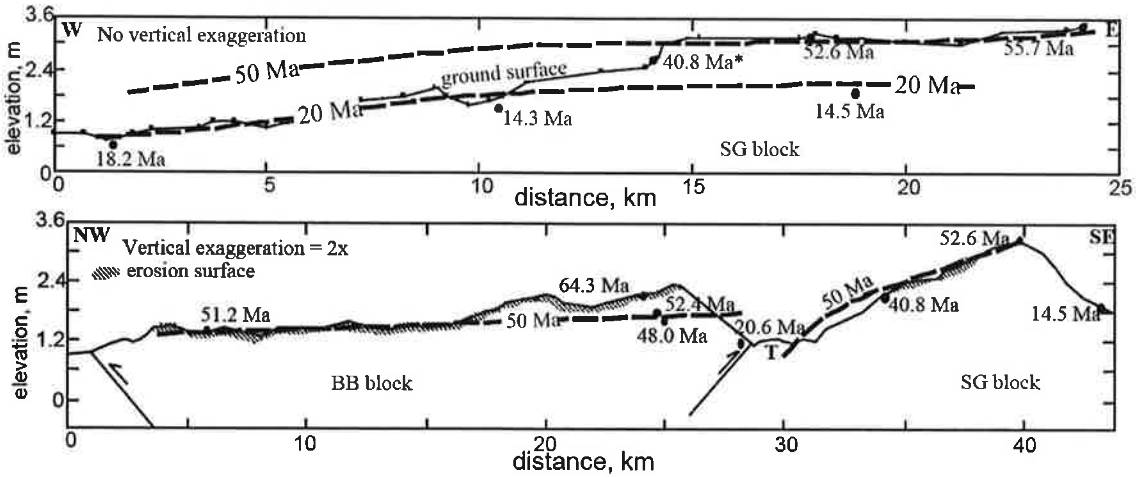

Figure 19. Profiles of apatite helum age isochrons (Ma) and weathered erosion surface patches in the San Bernardino Mountains (Spotila et al., 1998). Upper plot shows northwards view from west to east along the San Gorgonio block, illustrating that the block is a broad dome about a north-trending axis. The upper portion of the block has been minimally eroded (i.e. where ages are >50 Ma at the surface), but incision has caused younger ages to be exposed successively to the west. The lower plot shows both the Big Bear and San Gorgonio blocks along a NW-SE profile, looking to the east. The 50 Ma isochron along the San Gorgonio block plunges to the north beneath Barton Flats. The 50 Ma isochron and erosion surface in the Big Bear block show that the entire plateau has been minimally eroded and uplifted along opposed thrust faults.

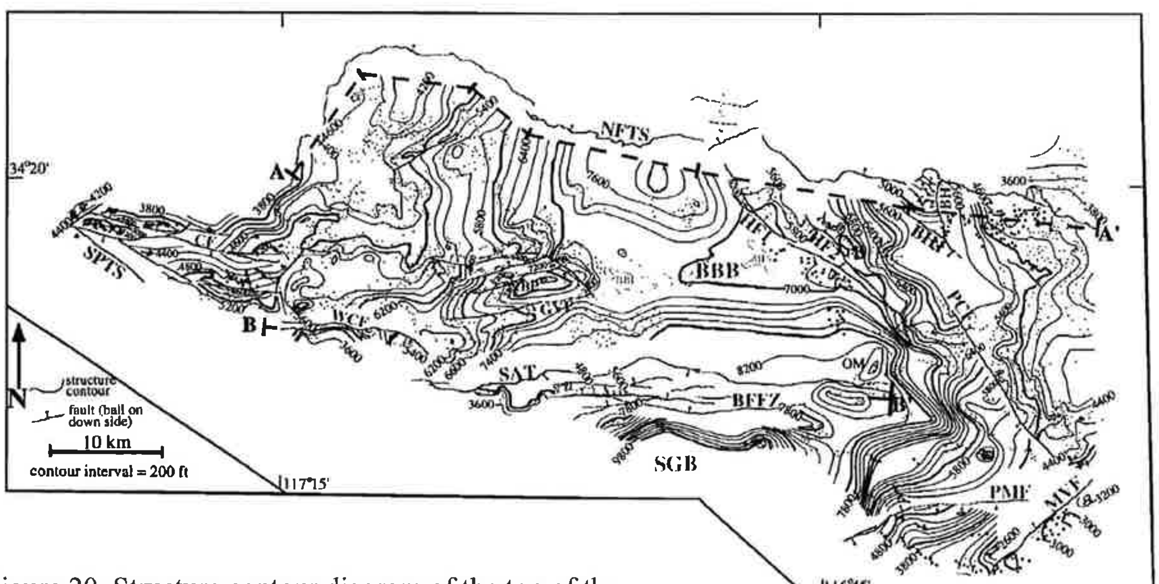

Figure 20. Structure contour diagram of the top of the deeply weathered erosion surface on the Big Bear block (BBB) and San Gorgonio block (SGB) (Spotila and Sieh, 2000). Elevations of contours are in feet. Dots indicate the locations used for observation of elevation from 1:62,500 scale topographic maps based on the surface as mapped using stereo air-photos. Although the overall pattern is somewhat irregular and locally offset by faults within the plateau (e.g. Pipes Canyon fault; PCF), the structure contour diagram reveals a broad domal form of the upper plateau surface. Other abbreviations: BFFZ – Barton Flats fault zone, BHF – Bighorn fault, CF – Cleghorn fault, GVF – Green Valley fault, HF – Helendale fault, MVF – Morongo Valley fault, NFTS – North Frontal thrust system, PMF – Pinto Mountain fault, SAT – Santa Ana thrust, WCF – Waterman Canyon fault.

Figure 21. Google-Earth image of some of the basalt-capped mesas at Pioneertown. Note the two flat basalt covered surfaces that overlie sandstone, that together are deposited on quartz monzonite. Where the overlying units and weathered granite are removed by erosion, the granite has the characteristic corestone expression (blue circled area). The average depth of incision since the Miocene along this flank of the plateau, where the plateau merges with the floor of the Mojave Desert, is ~150 m.

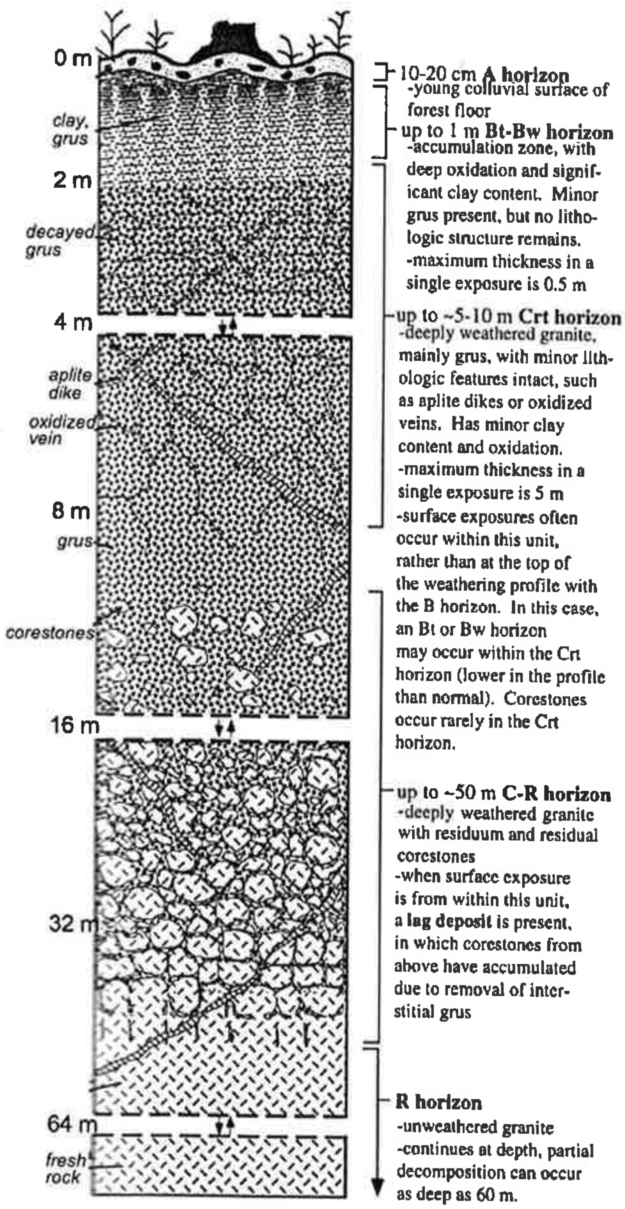

Figure 22. Schematic diagram of typical deeply weathered profile atop the Big Bear plateau erosion surface (Spotila, 1999).

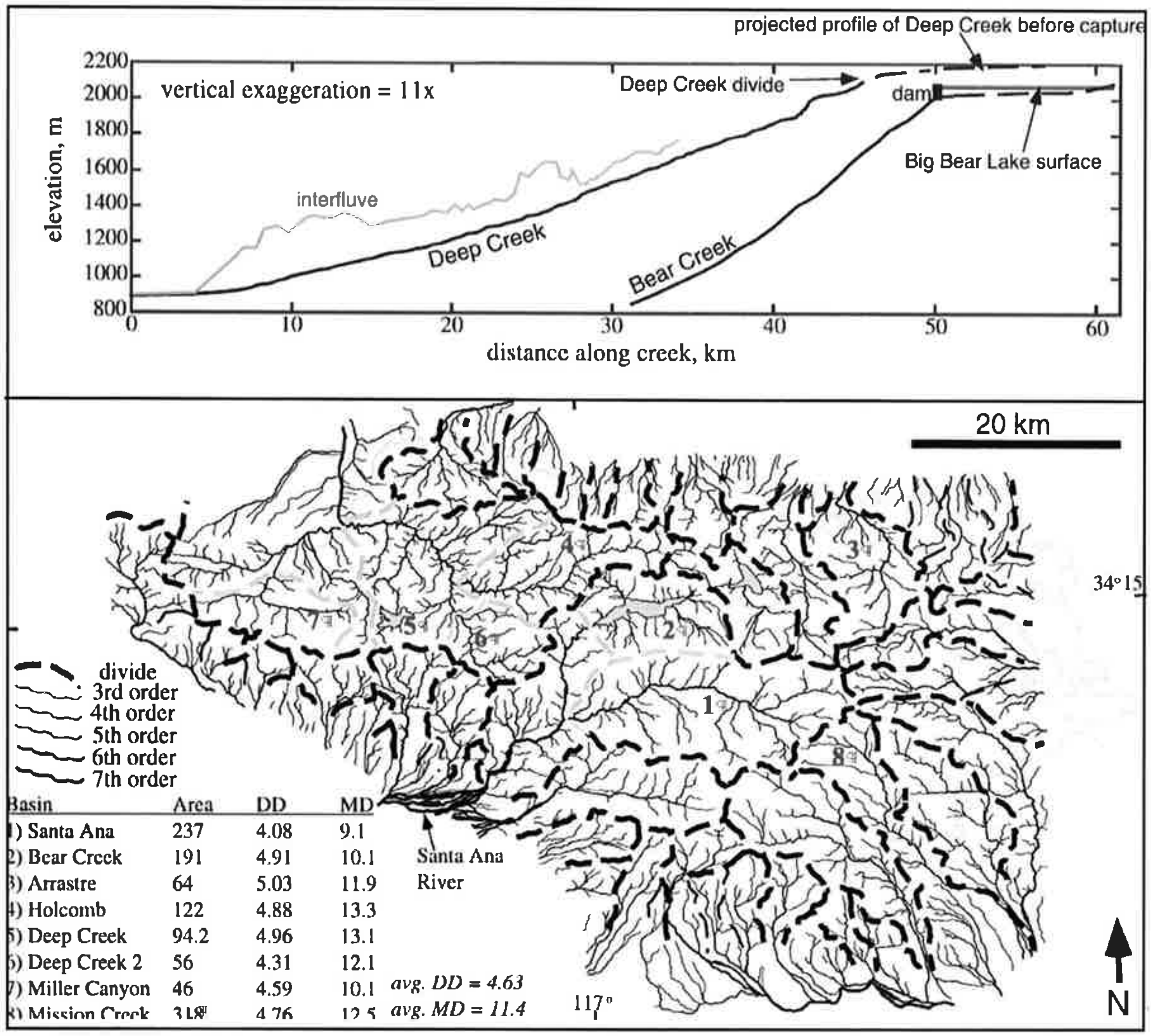

Figure 23. Stream profiles of rejuvenated Deep Creek, which lies in the northwestern part of the Big Bear plateau, and Bear Creek, which drains Big Bear Lake. The prominent knickpoint at the top of Bear Creek suggests stream capture. It is possible that the former network flowed to the WSW from Big Bear Lake, through the low region just north of Keller Peak, and connected up to the Deep Creek network. Bottom figure shows the drainage network of the entire range. DD = drainage density (km^2), MD = magnitude density. Both figures are from Spotila et al. (2002).

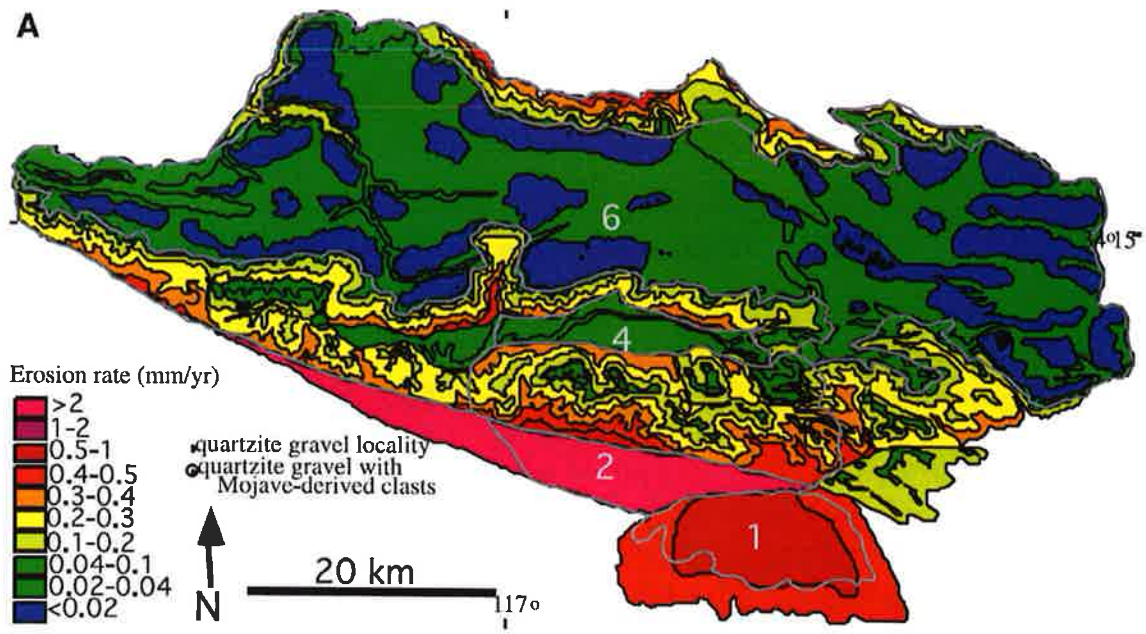

Figure 24. Erosion rate model for syn-uplift (post-2.5 Ma) denudation of the entire San Bernardino Mountains (Spotila et al., 2002

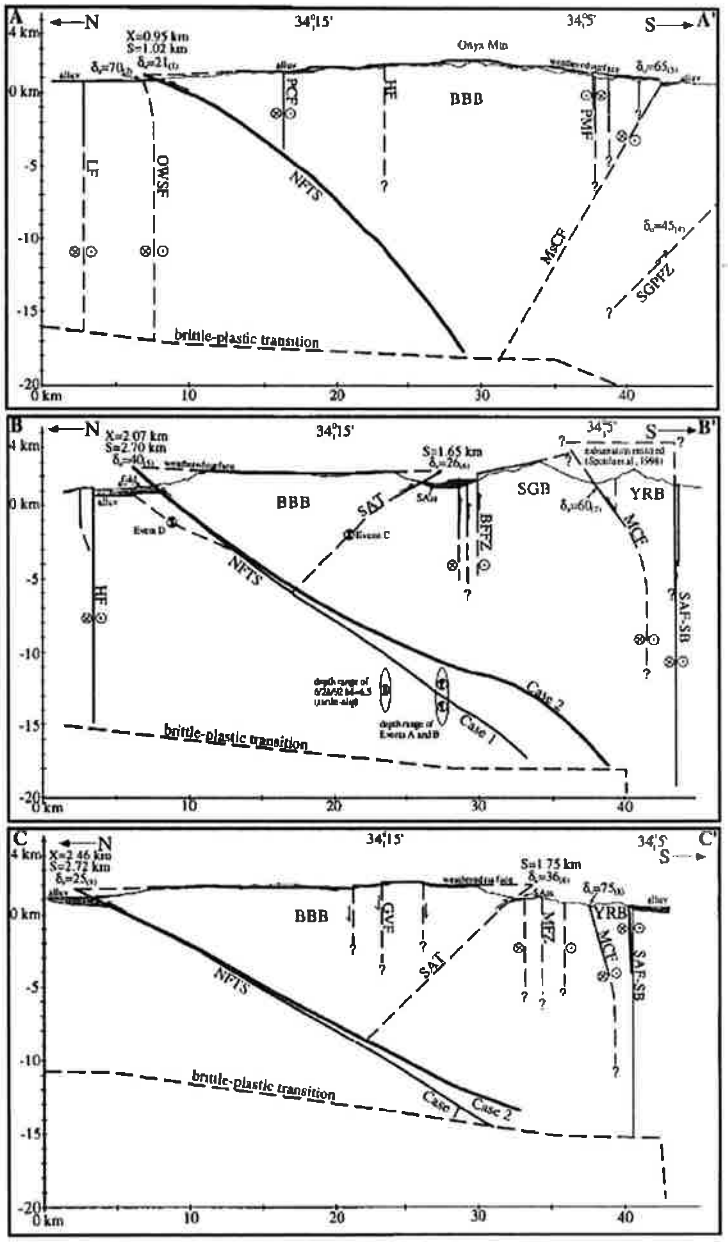

Figure 25. N-S cross sections across the San Bernardino Mountains, showing the interpreted geometry of the underlying North Frontal thrust system based on reconstruction and use as a datum of the weathered erosion surface atop the Big-Bear plateau. Location of sections shown in Figure 24. From Spotila and Sieh (2000).

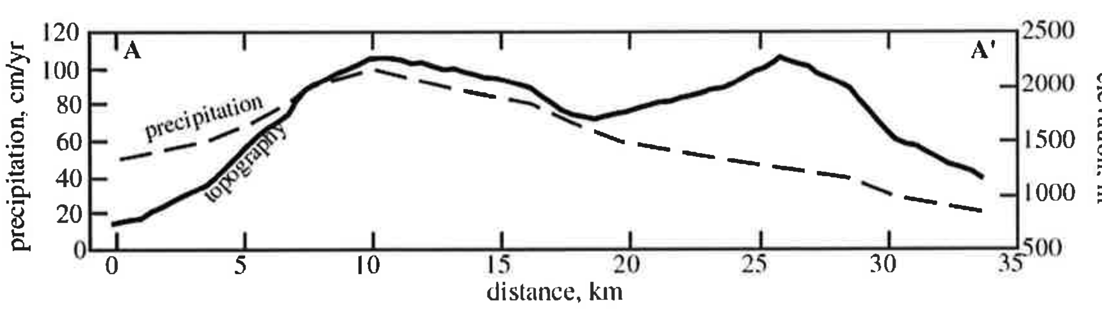

Figure 26. Orographic precipitation across the Big Bear plateau. Cross section extends from south to north (A to A'). Annual precipitation peaks along the southern escarpment and drops off quickly towards the Mojave Desert towards the north.

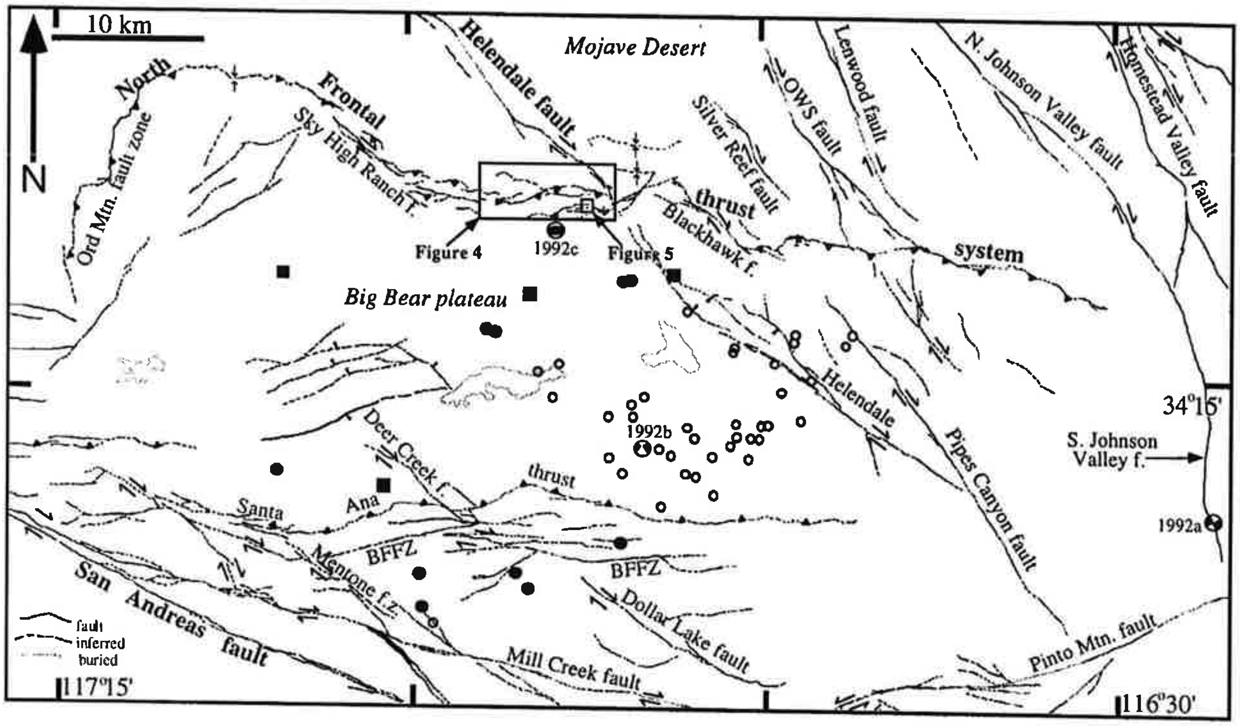

Figure 27. Map of major structures along the North Frontal thrust system (Spotila and Anderson, 2004). Open circles are M>4 events from the 1992 Big Bear sequence that could be produced by northwest trending dextral faulting. Closed circles and squares are M>4 events before and after that from NW-trending dextral ruptures.

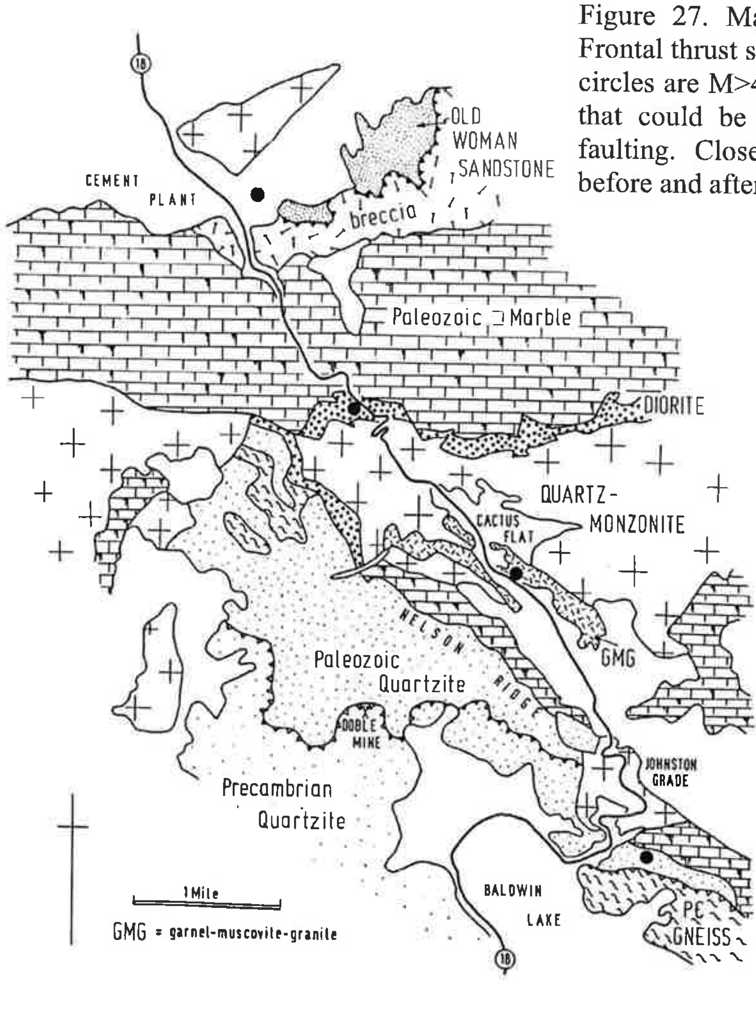

Figure 28. Generalized geologic map of the Johnston and Cushenbury Grades, from Sadler (1990).

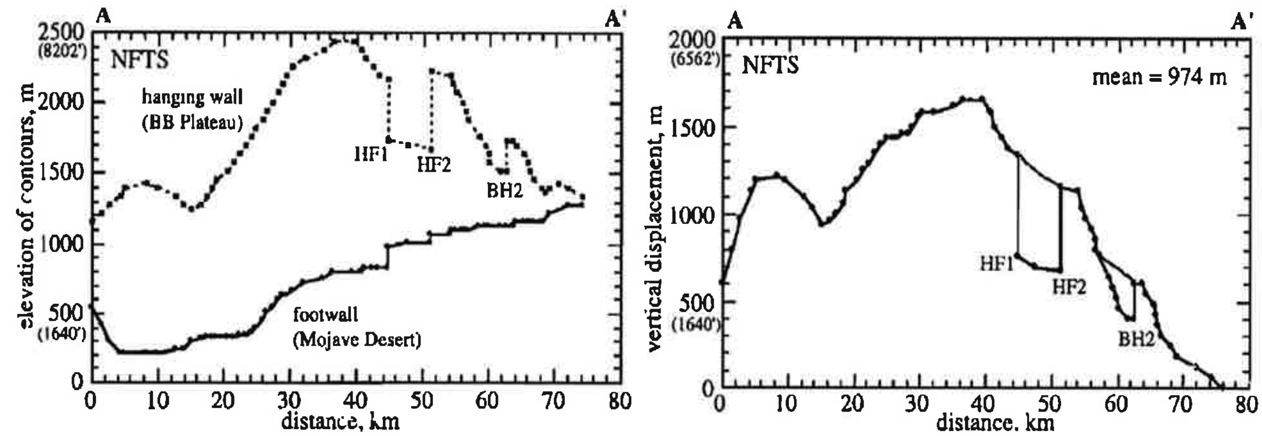

Figure 29. Plot of net vertical offset along the North Frontal thrust system based on reconstruction of the deeply weathered surface atop the plateau and its displacement above the top of basement buried in the thick alluvium along the northern range front in the Mojave Desert. Note how the offset along the thrust is cut by the strands of the Eastern California shear zone (Helendale and Bighorn faults). From Spotila and Sieh (2000).

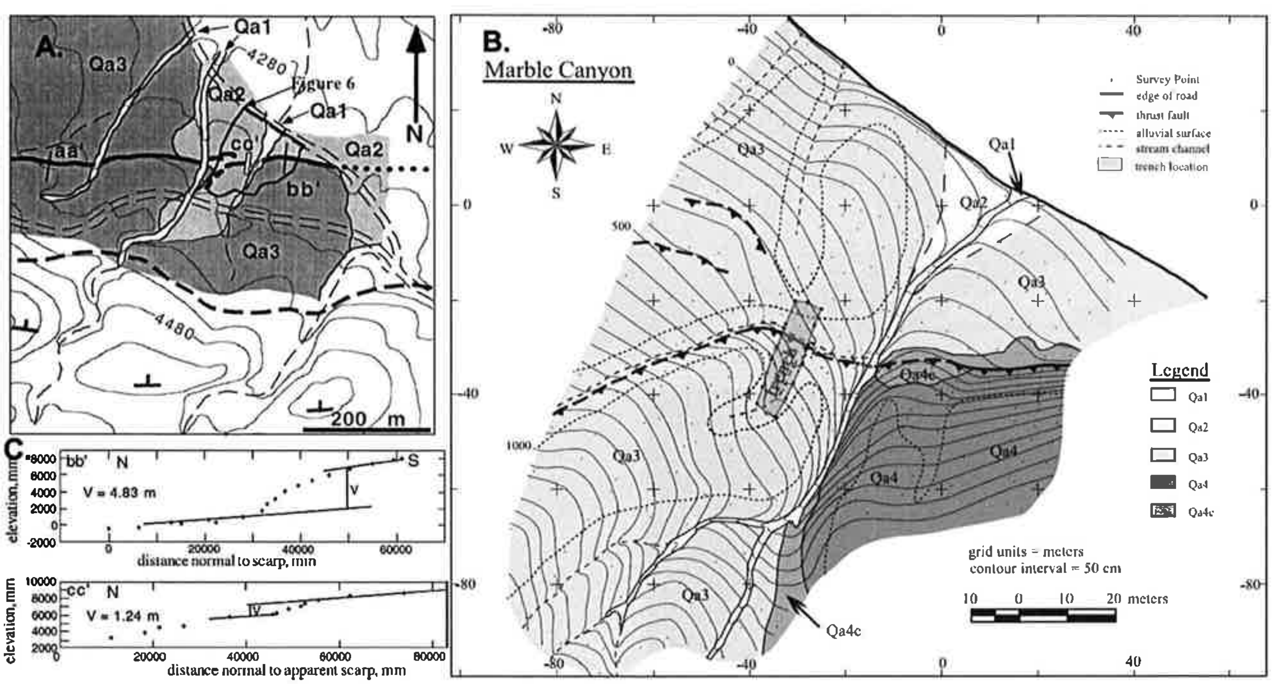

Figure 30. A) Geomorphic map of the NFTS to the west of the Helendale fault. The thrust trace includes older faults and folds to the north and south, and a youthful trace in Pleistocene alluvium (Qa3) with a 5-8 m high scarp. A smaller, 1-2 m, subdued scarp occurs in younger alluvium (Qa2) and was trenched. B) Detailed topographic map of trench location across the NFTS. C) Topographic profiles across scarps developed in older and younger alluvium (lines BB' and CC', shown in A).

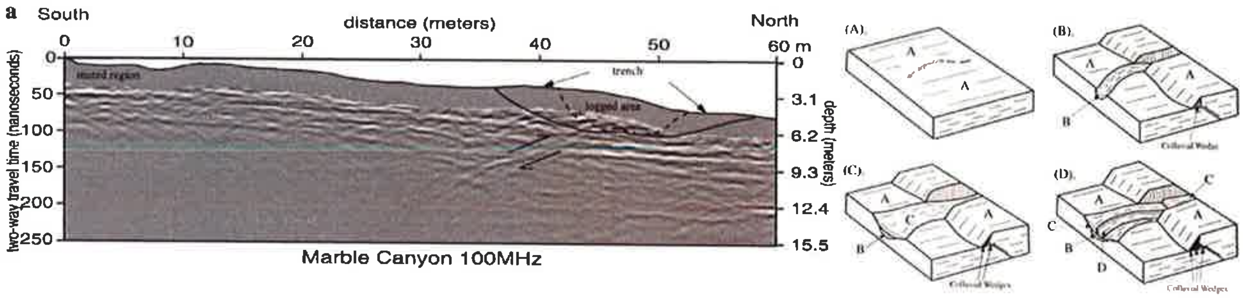

Figure 31. GPR profile across trench site shown in Figure 30. Note that a prominent south-dipping reflector intersects the thrust trace, showing that GPR is a useful geophysical tool for pre-trench neotectonic characterization in this setting. The cartoon to the right illustrates the characteristics of a good paleoseismic site in this tectonic environment. Rather than trenching the high scarps in older alluvium, which may not preserve a history of rupture events, it is better to trench in younger alluvium where the main scarp has been incised. Following this technique along the NFTS revealed a Holocene offset (from Anderson et al., 2003).

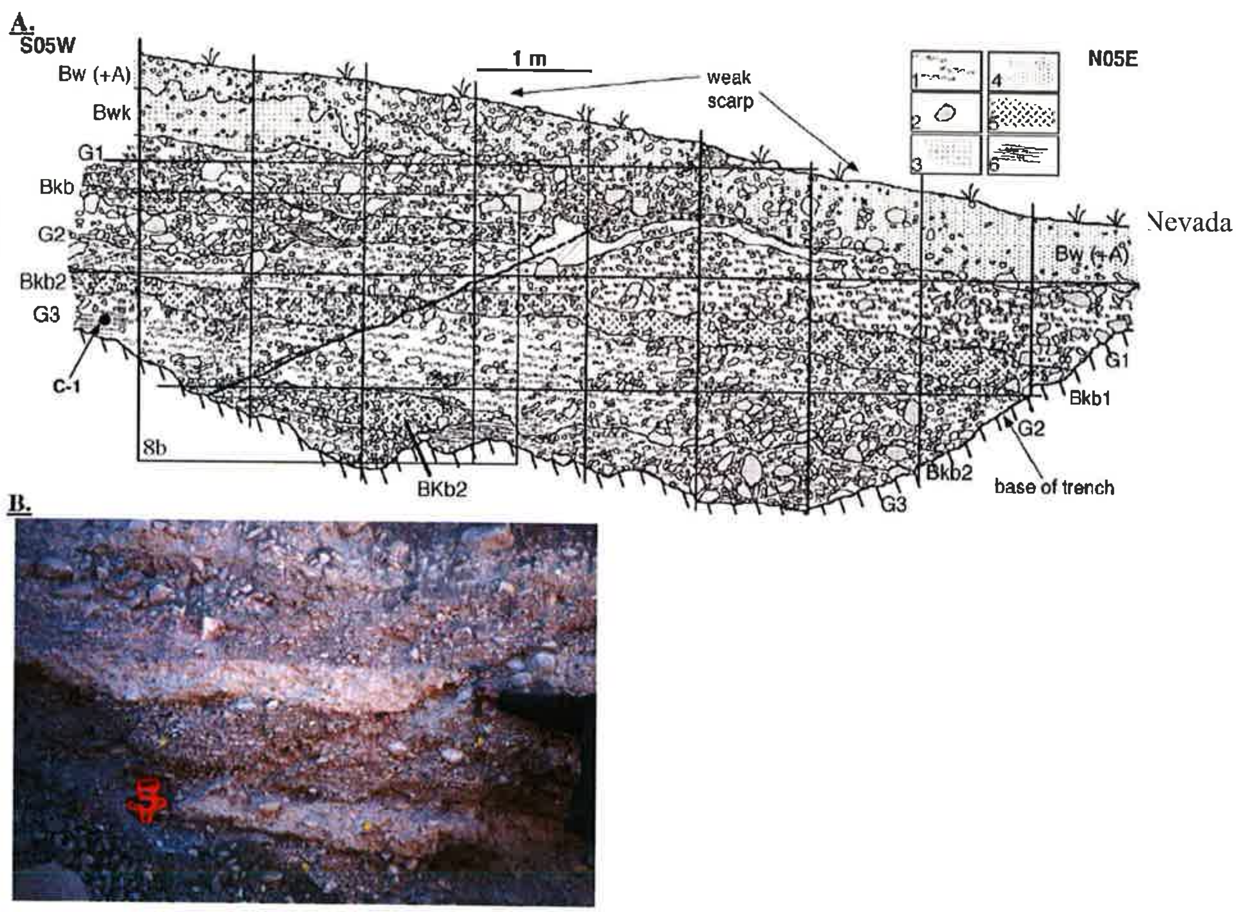

Figure 32. Log and photograph of the trench shown in Figure 31. A 20-m-long, 3-m deep bulldozer cut revealed this offset stratigraphy. Offset defined by white paleosols in the photograph is 1.7 m on a 23° south-dipping plane. The radiocarbon age of bulk carbon at C-1 (11,160 years BP) indicates that this thrusting event was likely Holocene in age, showing that the NFTS, at least here, is still active.

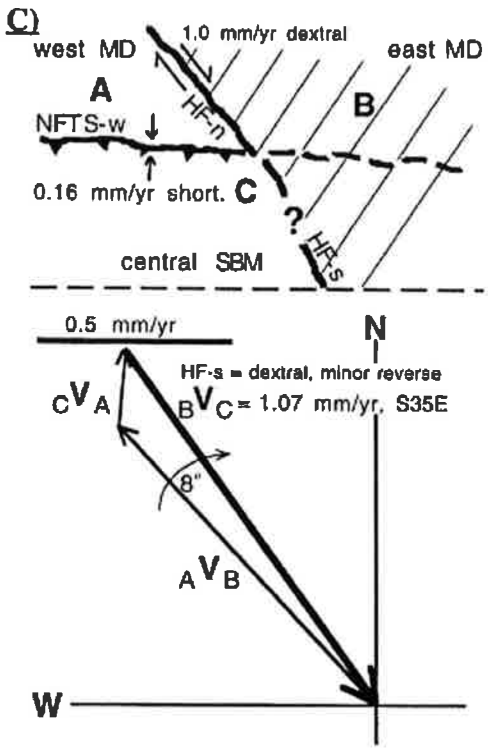

Figure 33. Velocity model for the confluence of the Helendale and North Frontal thrust system. This model assumes the eastern NFTS is inactive. Assuming 1 mm/yr on the northern Helendale fault and 0.16 mm/yr shortening on the NFTS (observed in the trench), the southern Helendale fault in the hanging wall would have 1.07 mm/yr oblique dextral-reverse slip along a slightly more northerly-trending plane.

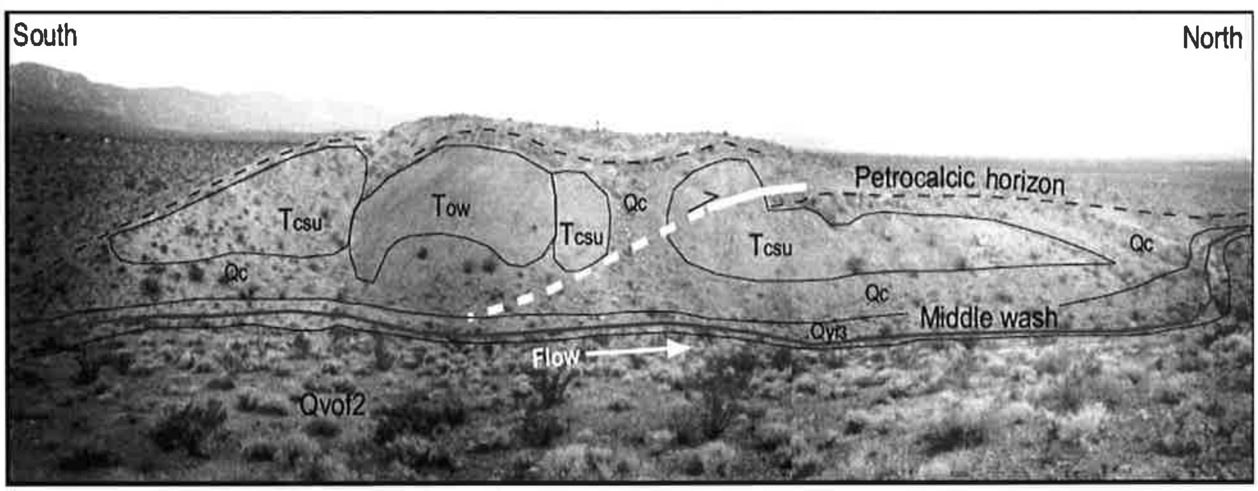

Figure 34. View to the west of incision into the core of the Cougar Buttes anticline (from Pearce et al., 2004). Tcsu = Cushenbury Springs formation, Tow = Old Woman sandstone.

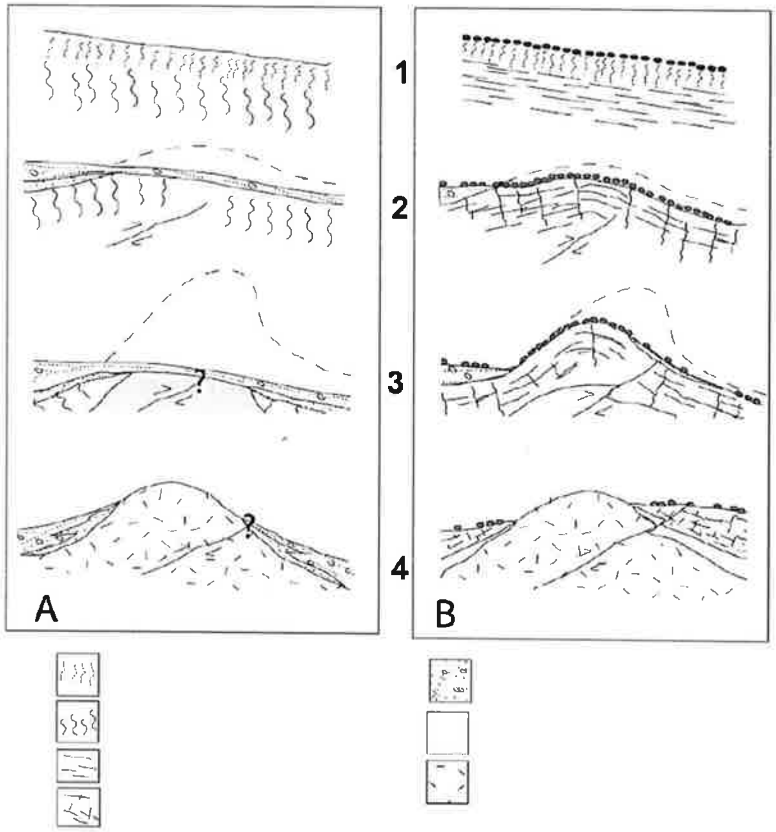

Figure 35. Conceptual model of fold development along the range front as influenced by the differential erodibility of soils developed on granitic (A) versus limestone-rich (B) alluvium (from Eppes et al., 2002). In the progressive stages of development, petrocalcic horizons armor the folds in limestone-rich alluvium, resulting in growth of prominent ridges in the foreland, whereas folds in granitic alluvium are easily eroded and will remain masked until cored by basement.

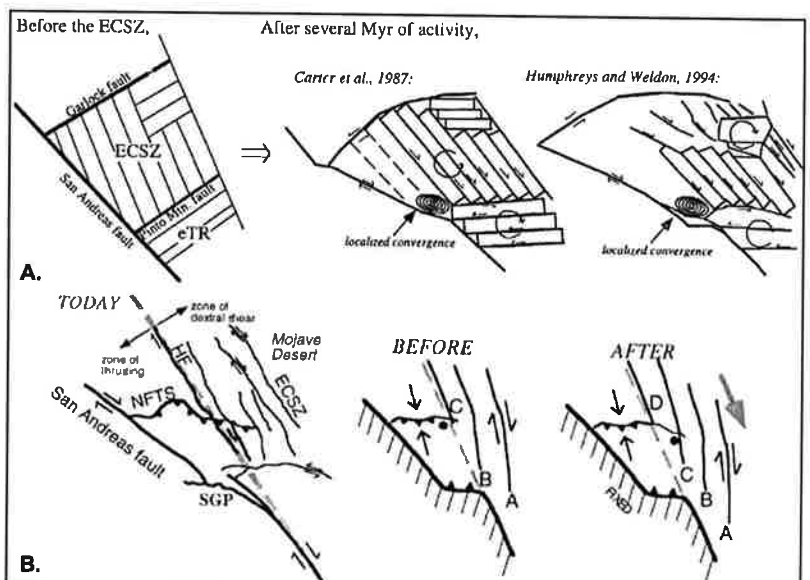

Figure 36. A) Model of rotation of the Mojave (ECSZ) and eastern Transverse Ranges (eTR) via bookshelf faulting, and formation of a deflection in the San Andreas fault at San Gorgonio Pass, localized at the boundary between these rotational domains at the Pinto Mountain fault (Spotila and Sieh, 2000). B) Model of progressive migration of the ECSZ to the west, as the San Bernardino Mountains move slowly to the east due to motion along the San Andreas fault. This implies that the range is not totally fixed relative to the bend at San Gorgonio Pass, but has migrated slightly during its 2.5 Myr history (Spotila and Anderson, 2004).